High fat diet promotes obesity by driving miRNA dependent neurogenesis and integration of orexigenic neurons in the feeding circuitry

Balakumar Srinivasan[1], Sarbani Samaddar[1], Himanshu Singh[3], Senthil Kumaran[3], Dipanjan Roy[1, 2], and Sourav Banerjee[1]

1. National Brain Research Centre, NH8, Nainwal Mode, Manesar 122052, Haryana, INDIA
2. Current address: School of Artificial Intelligence and Data Science, Indian Institute of Technology, Jodhpur 342030, Rajasthan, INDIA
3. Department of NMR and MRI Facility, All India Institute of Medical Sciences, Ansari Nagar, New Delhi 110029, INDIA

Corresponding Author: Sourav Banerjee

Correspondence: souravnbrc@gmail.com or sourav@nbrc.ac.in

Author Contributions: Conceptualization: Sourav Banerjee

Data curation: Balakumar Srinivasan, Sarbani Samaddar, Himanshu Singh

Data analysis: Balakumar Srinivasan, Sarbani Samaddar, Himanshu Singh

Writing – original draft: Balakumar Srinivasan, Sarbani Samaddar, Sourav Banerjee

Writing – review & editing: Sarbani Samaddar, Sourav Banerjee

Funding acquisition: Sourav Banerjee.

Competing Interest Statement: Authors declare no competing interests.

Keywords: miRNAs; Hypothalamus; Tanycytes; Adult Neurogenesis; High Fat Diet.

Data Availability: All data and codes used for analysis are available at https://figshare.com/s/abef061d9d61a06f3dd7

Abstract

A high-fat diet (HFD) regulates the feeding circuitry in young-adult mice by stimulating neurogenesis from β2 tanycytes in the hypothalamus. However, the fate of HFD-induced tanycytic neurogenesis, the functional attributes of the nascent neurons, and mechanisms underlying their subsequent integration into the feeding-related neural circuitry remain unclear. microRNAs (miRNAs) are known to play crucial roles in adult neurogenesis. In this study, miRNA profiling of BrdU-labelled neurogenic β2 tanycytes from HFD-fed mice identified a cohort of miRNAs that originate from different chromosomal loci rather than a single genomic cluster. Network analysis of predicted targets for these HFD-induced miRNAs identified key "hub" mRNA targets that influence neurogenesis and the functional integration of newborn neurons. These HFD-induced miRNAs promoted the differentiation of nascent neurons into orexigenic AgRP+ and anorexigenic $POMC^{+}$ neurons. Interestingly, only AgRP+ newborn neurons were selectively integrated into the functional feeding circuit, as detected by c-Fos immunostaining. This integration was disrupted when HFD-induced miRNA activity was suppressed via hypothalamic miRNA sponge expression. Furthermore, HFD feeding increased body weight in female mice, which was abrogated upon the inhibition of HFD-induced miRNAs. Magnetic resonance imaging (MRI) revealed elevated liver fat in HFD-fed mice, which reverted to normal levels when the HFD-induced miRNAs in hypothalamic tanycytes were blocked. Collectively, the findings from our study highlight a miRNA-mediated paradigm that links HFD-induced neurogenesis from β2 tanycytes to weight gain and liver fat accumulation, and identifies the selective integration of AgRP+ neurons into the feeding circuitry as a possible causality of HFD-induced changes to body weight.

Significance Statement

This study highlights a miRNA-network that biases the transcriptional program in hypothalamic tanycytes to promote neurogenesis in young adult mice following their exposure to an acute high-fat diet (HFD) paradigm. These HFD-induced miRNAs have the potential to alter the brain's feeding circuitry by promoting neurogenesis and the preferential functional integration of nascent orexigenic (AgRP+) neurons; resulting in weight gain and hepatic fat accumulation. Collective inhibition of this miRNA-network prevents the integration of newborn AgRP+ neurons and reverses the metabolic consequences of high-fat diet. Our study provides an unexplored link between diet, neurogenesis, and remodeling of the feeding circuitry; and reveals potential therapeutic targets for combating hyperphagic obesity.

Main Text

Introduction

Research on adult neurogenesis has extended beyond the classical regions of the subventricular zone and the subgranular zone to include roles of other neurogenic niches in the adult mouse brain (1–3). Particularly, there has been a growing interest in hypothalamic neurogenic niches; their responsiveness to dietary factors further underscores their critical role in metabolic and physiological regulation. Hypothalamic adult neurogenesis in response to acute or sustained dietary changes modulate long-term physiological responses in the body such as aberrant body fat regulation and obesity. Studies show that adult neurogenesis from different niches of the brain occur in concomitance with weight gain in mice exposed to both acute and chronic high fat diet (HFD), though the nature of obesity differs between these feeding paradigms (4, 5). Chronic HFD consumption results in severe obesity (6, 7), whereas acute HFD intake induces reversible weight gain (8).

Acute HFD feeding stimulates neurogenesis in the hypothalamic median eminence (MEm) of adult mice (5). This region contains an active neurogenic niche marked by the presence of Nestin+, radial glia-like ependymal cells called tanycytes (9). Tanycytes are metabolite sensing ependymal cells lining the ventral third ventricular wall; anatomically characterized into α1-, α2-, β1-, and β2-subtypes. They are capable of sensing metabolites from the cerebrospinal fluid and blood due to their position outside the blood-brain barrier and have characteristically long projections to the dorsomedial hypothalamus, ventromedial hypothalamus, arcuate nucleus (ArcN) and the median eminence (MEm) (9). Neural circuits underlying feeding behaviour in the mouse brain is centralized to the ArcN, which integrates opposing feeding signals due to the presence of two neuron types: anorexigenic POMC+ neurons promoting satiety, and orexigenic AgRP+ neurons that drive hunger (10–12). AgRP+ and POMC+ neurons are dimorphic and they reciprocally inhibit each other (12). β1-and β2-tanycytes relay signals to activate the ArcN feeding circuits (13, 14) and therefore influence the function of both AgRP+ and POMC+ neurons. β2-tanycytes are Sox2+/Nestin+/Vimentin+ diet-responsive neural progenitors that adapt to a neural fate in response to variations in dietary factors (5). Neurogenesis from β2-tanycytes is critical for HFD-induced metabolic adaptation in female mice; previous studies report that irradiation of the MEm ablates β2-tanycytes and prevents HFD-driven weight gain (5). However, how HFD-induced neurogenesis occurs from β2-tanycytes and how these nascent neurons are integrated into the feeding circuit is unknown.

Among the various effectors influencing diet-induced modulation of the hypothalamic feeding circuits, miRNAs play a unique but understudied role. These small noncoding RNAs modulate mRNA translation and RNA stability in response to external cues, positioning them as likely

90 regulators of metabolic pathways during both acute and chronic dietary changes. Studies confirm
91 that hypothalamic miRNA expression changes due to both acute and chronic nutritional
92 interventions in rats (15, 16), with specific miRNAs (let-7a, miR-9, miR-30e, miR-103, miR-132, miR-
93 145, miR-200a, miR-218) responding to either calorie restriction or HFD. Notably, administration of
94 miR-103-mimic to the ArcN of Dicer KO mice attenuated hyperphagic obesity (16). miRNAs are
95 also established regulators of adult neurogenesis from the subventricular zone of the lateral
96 ventricle and the subgranular zone of the hippocampus (17, 18). Thus, miRNAs likely mediate HFD-
97 induced tanycytic neurogenesis and subsequent circuit modifications (18–23), bridging dietary
98 inputs to neural adaptations.

99 In this study, we profiled miRNAs in BrdU+ β2-tanycytes from female C57BL/6j mice after acute
100 HFD exposure, identifying a cohort of diet-induced miRNAs. By conducting a protein–protein
101 interaction network analysis for proteins encoded by mRNAs that are targeted by this collective
102 cohort of miRNAs, we uncovered a miRNA-mediated molecular framework involved in HFD-
103 induced neurogenesis from β2-tanycytes. Fate-mapping demonstrated differentiation of the
104 nascent neurons into both orexigenic AgRP+ and anorexigenic POMC+ types, but only AgRP+
105 neurons showed functional circuit integration as evidenced by c-Fos expression. Inhibition of HFD-
106 induced miRNAs in the hypothalamus disrupted this neuronal integration, which in turn reversed
107 HFD-induced body weight gain. Magnetic resonance imaging (MRI) indicates that suppressing
108 these miRNAs also inhibited the accumulation of liver fat. Our findings unveil an unexplored miRNA-
109 dependent mechanism regulating body weight through hypothalamic neurogenesis and selective
110 orexigenic neuron recruitment into the feeding circuit in female mice following acute exposure to
111 a high-fat diet.

112 **Results**

113 **HFD induces the upregulation of a cohort of miRNAs in neurogenic β2 tanycytes.**

114 To identify diet-regulated miRNAs from neurogenic tanycytes present in the median eminence
115 (MEm), female mice were either given normal chow diet (NCD) or HFD during P45 – P75 and
116 tanycytes undergoing neurogenesis were labelled by BrdU incorporation (Fig. 1A). Female mice
117 were specifically used for this study as previous research has demonstrated that the median
118 eminence of female, but not male, mice showed enhanced neurogenesis after HFD feeding (8).
119 Using laser capture microscopy, $BrdU^+$ tanycytes (Fig. 1B) were isolated from the median eminence
120 and the differential expression of miRNAs were analyzed by miRNA arrays. We observed that 32
121 miRNAs were differentially expressed upon HFD feeding, whereas 5 miRNAs were differentially
122 expressed in NCD fed mice. Among these transcripts, a cohort of miRNAs; miR-382, miR-145,

123 miR-196, miR-1894 and let-7b (Table 1) were significantly up-regulated upon HFD feeding (Fig.
124 1C); whereas NCD feeding significantly enhanced the expressions of let-7d, let-7i and let-7e

A.

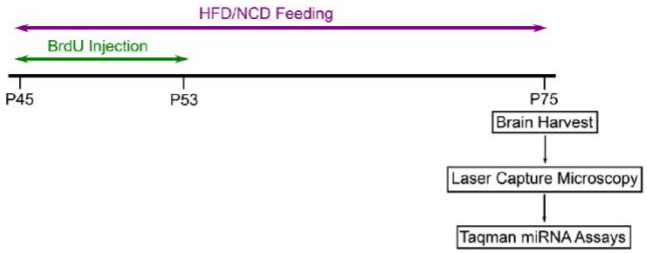
HFD/NCD Feeding
BrdU Injection
P45
P53
P75
Brain Harvest
Laser Capture Microscopy
Taqman miRNA Assays

B.

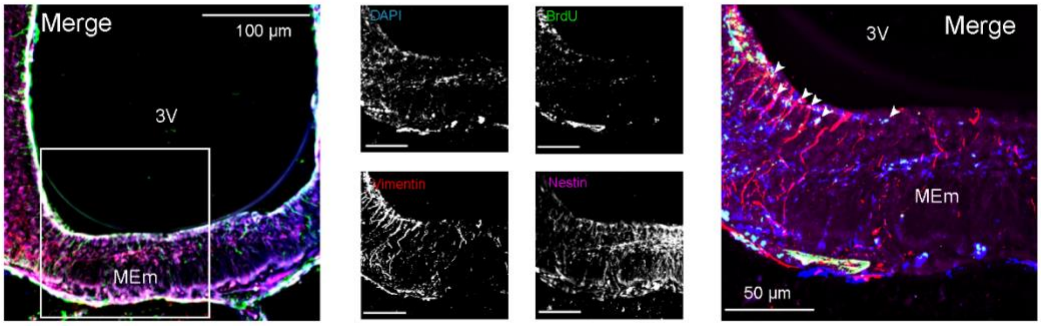
Merge
100 µm
3V
MEm
DAPI
BrdU
Vimentin
Nestin
3V
Merge
MEm
50 µm

C.

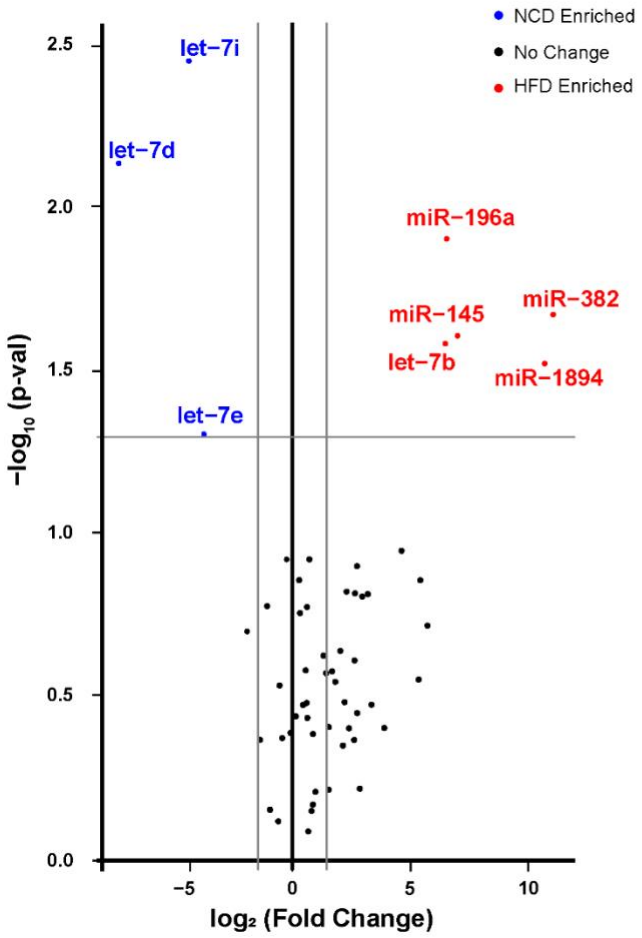
NCD Enriched
No Change
HFD Enriched
let−7i
let−7d
let−7e
miR−196a
miR−145
let−7b
miR−382
miR−1894
−log10 (p-val)
log2 (Fold Change)
2.5
2.0
1.5
1.0
0.5
0.0
−5
0
5
10

D.

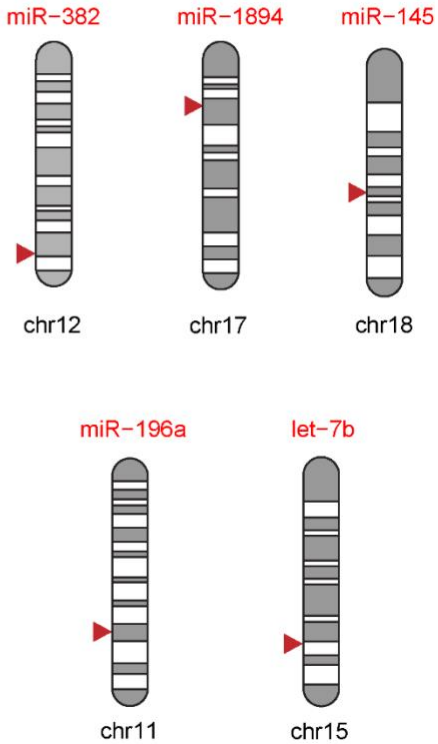
miR−382
miR−1894
miR−145
chr12
chr17
chr18
miR−196a
let−7b
chr11
chr15

126 **Fig. 1: Differentially expressed miRNAs identified from adult neurogenic tanycytes in**
127 **median eminence.**

128 (A) Experimental paradigm to determine the miRNA expression profiles by isolation of BrdU
129 labelled β2 neurogenic tanycytes of the median eminence. (B) Photomicrograph showing BrdU
130 labelling of Nestin^{+} and Vimentin^{+} β2 neurogenic tanycytes in median eminence (MEm) post 30
131 days of HFD feeding. (C) Scatter volcano plot showing expression of miRNAs from β2 neurogenic
132 tanycytes following HFD (red) or NCD (blue) feeding. Significant changes in miRNA expression
133 (marked by arrow). N = 3 independent experiments. Two-tailed t-test was performed and post hoc
134 false discovery rates (FDR) was analyzed using the Benjamini-Hochberg method. ArcN: Arcuate
135 Nucleus, 3V: Third ventricle, MEm: Median Eminence. Scale bars are as indicated. (D) Karyotype
136 Phenogram shows the genomic locations of differentially expressed miRNAs.

137 (Table 1) (Fig. 1C). Interestingly, these miRNAs are not localized to a single genomic cluster, rather
138 they originate from different chromosomes (Fig. 1D). Our results indicate that miRNAs are
139 differentially expressed in the neurogenic β2-tanycytes of female mice following acute exposure to
140 HFD.

141 **Diet-induced miRNAs regulate a network of transcripts involved in neurogenesis.**

142 To determine how miRNAs regulate the neurogenesis from β2 tanycytes, mRNA targets of the
143 HFD-responsive miRNAs; miR-1894, miR-382, miR-145, miR-196 and let-7b were analyzed. We
144 reasoned that since miRNAs exert regulatory control on the translation or stability of mRNAs, the
145 mRNAs that would be most affected due to HFD are likely to possess binding sites for all five HFD-
146 induced miRNAs. Accordingly, putative target mRNAs containing binding sites for all five miRNAs
147 were obtained from the TargetScan, miRdb and PicTar databases. We have selected 1204
148 transcripts represented in all three databases and analyzed the interactions between them using
149 StringDB. Graph theory-based network analysis was performed to determine the key miRNA target
150 transcripts. Nodes (mRNA targets) were clustered using Louvain's community clustering method
151 (24). Stable optimization of the clustering of the nodes using the above method was achieved using
152 a resolution parameter ranging from 0.5 – 0.75 (Fig. 2A). We observed a highly modular network
153 among the targets of the upregulated miRNAs upon HFD feeding, whereas this modularity is absent
154 upon NCD feeding. We have detected 11 modules in the HFD network, out of which 6 modules are
155 highlighted (Fig. 2B). This network modularity is a key target selection criterion for further analysis
156 as clustered transcripts within a network have the potential to work concertedly to drive
157 neurogenesis in the tanycytes

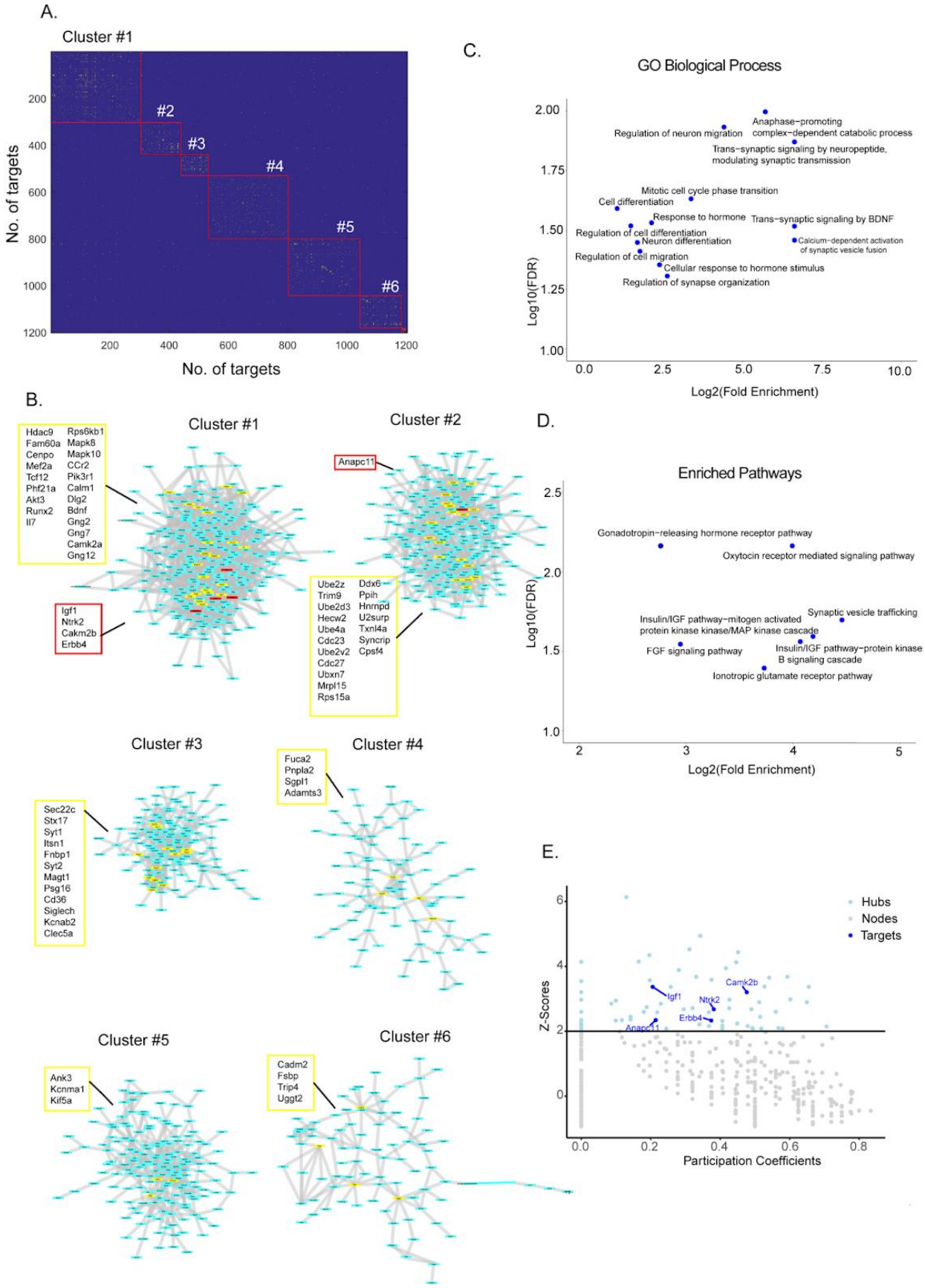
A.
Cluster #1
#2
#3
#4
#5
#6
No. of targets
No. of targets
B.
Cluster #1
Hdac9 Rps6kb1
Fam60a Mapk8
Cenpo Mapk10
Mef2a CCr2
Tcf12 Pik3r1
Phf21a Calm1
Akt3 Dlg2
Runx2 Bdnf
Il7 Gng2
Gng7
Camk2a
Gng12
Igf1
Ntrk2
Cakm2b
Erbb4
Cluster #2
Anapc11
Ube2z Ddx6
Trim9 Ppih
Ube2d3 Hnrnpd
Hecw2 U2surp
Ube4a Txnl4a
Cdc23 Syncrip
Ube2v2 Cpsf4
Cdc27
Ubxn7
Mrpl15
Rps15a
Cluster #3
Sec22c
Stx17
Syt1
Itsn1
Fnbp1
Syt2
Magt1
Psg16
Cd36
Siglech
Kcnab2
Clec5a
Cluster #4
Fuca2
Pnpla2
Sgpl1
Adamts3
Cluster #5
Ank3
Kcnma1
Kif5a
Cluster #6
Cadm2
Fsbp
Trip4
Uggt2
C.
GO Biological Process
Anaphase−promoting complex−dependent catabolic process
Regulation of neuron migration
Trans−synaptic signaling by neuropeptide, modulating synaptic transmission
Mitotic cell cycle phase transition
Cell differentiation
Response to hormone
Trans−synaptic signaling by BDNF
Regulation of cell differentiation
Neuron differentiation
Calcium−dependent activation of synaptic vesicle fusion
Regulation of cell migration
Cellular response to hormone stimulus
Regulation of synapse organization
Log10(FDR)
Log2(Fold Enrichment)
D.
Enriched Pathways
Gonadotropin−releasing hormone receptor pathway
Oxytocin receptor mediated signaling pathway
Synaptic vesicle trafficking
Insulin/IGF pathway−mitogen activated protein kinase kinase/MAP kinase cascade
FGF signaling pathway
Insulin/IGF pathway−protein kinase B signaling cascade
Ionotropic glutamate receptor pathway
Log10(FDR)
Log2(Fold Enrichment)
E.
Hubs
Nodes
Targets
Igf1
Camk2b
Ntrk2
Erbb4
Anapc11
Z-Scores
Participation Coefficients

Fig. 2: Weighted gene coexpression network analysis of target transcripts containing binding sites of HFD-regulated miRNAs.

(A) Adjacency matrix showing community clustering (red boxes) based on the interaction between each target as a node. (B). 6 clusters of the network of target transcripts containing binding sites for all five miRNAs. All hubs are indicated in the "yellow" box. Hubs selected for target validation via reporter assay are represented in the "red" box. (C) Scatter plots showing fold enrichment of significant GO-terms in Biological Process. (D) Scatter plots showing fold enrichment of significant GO-terms from pathway analysis. (E) Scatter plot showing the z-scores and the participation coefficients for all nodes in the network. Nodes are considered "hubs" for z-score > 2. Hubs selected for reporter analysis are indicated.

and subsequent neuronal differentiation upon HFD feeding. Among the modularized community clusters, inter-community and intra-community measures of nodal activity were analyzed to determine the important target nodes that are critical for the entire network. Participation coefficient, a marker for inter-community interactions, was analyzed for all nodes to define the hubs. We have analyzed z-scores, a marker for intra-community interactions, to select the critical hubs in the network. Hubs with z-scores > 2 were selected for Gene Ontology (GO) analysis. We reasoned that these hubs contain key transcripts that can regulate multiple nodes. mRNA targets that are positioned at the "hubs" of the network, are considered to be central effectors of diet induced neurogenesis and neuronal differentiation. GO analysis of the mRNA targets revealed significantly enriched GO-terms including neuron differentiation, mitotic cell cycle phase transition, cellular response to hormone stimulus, trans-synaptic signaling by BDNF, trans-synaptic signaling by neuropeptide modulating synaptic transmission, regulation of cell migration and anaphase-promoting complex-dependent catabolic (Table 1) (Fig. 2C). We have also assessed significant GO-enriched pathways that includes insulin/IGF pathway-protein kinase B signaling cascade, insulin/IGF pathway-mitogen activated protein kinase cascade, ionotropic glutamate receptor pathway, FGF-signaling pathway and gonadotropin-releasing hormone receptor pathway (Table 1) (Fig. 2D). Based on the GO-enrichment analysis, we have selected IGF1, NTRK2, CAMK2B, ERBB4 and ANAPC11 (Table 1) for further validation *in vitro* using a reporter assay (Fig. 2E).

HFD-induced miRNAs directly bind to the 3' UTR of mRNAs that are the central effectors of neurogenesis.

To experimentally validate the interactions between HFD-regulated miRNAs and their "hub" mRNA targets identified in our network analysis, we performed a luciferase reporter assay following the inhibition of all five HFD-induced miRNAs. The key hub transcripts IGF1, NTRK2, CAMK2B, ERBB4 and ANAPC11 were selected for the validation of miRNA-mRNA interactions *in vitro*; owing to their previous implications in neurogenesis (IGF1), neuronal development (ANAPC11, IGF1), synaptogenesis (CAMK2B,ERBB4), energy homeostasis (NTRK2) or hyperphagic obesity (NTRK2) (25–36).

196 To sequester five miRNAs simultaneously, a miRNA sponge (containing complementary binding
197 sites to all five miRNAs) was cloned into an AAV vector that co-expressed tdTomato (Fig. 3A). The
198 efficacy of the miRNA sponge was determined by the fluorescence intensity of tdTomato
199 expression. Administration of the miRNA sponge significantly reduced the intensity of tdTomato
200 expression (65.05% ± 12.52% decrease, $p<0.0001$) (Fig. S1B- S1C) as compared to that in the
201 control vector. The 3'UTRs of each target mRNA containing the binding sites of all five miRNAs
202 were fused to the Gaussia luciferase reporter (Fig. 3B). We co-transfected the miRNA sponge along
203 with each of the reporters in Neuro-2a cells. Simultaneous inhibition of all five HFD-induced
204 miRNAs led to the significant enhancement of luciferase reporter activity driven by the 3'UTRs of
205 IGF1, NTRK2, CAMK2B and ERBB4 (Fig. 3C); but not ANAPC11 (Table 1) (Fig. 3C).

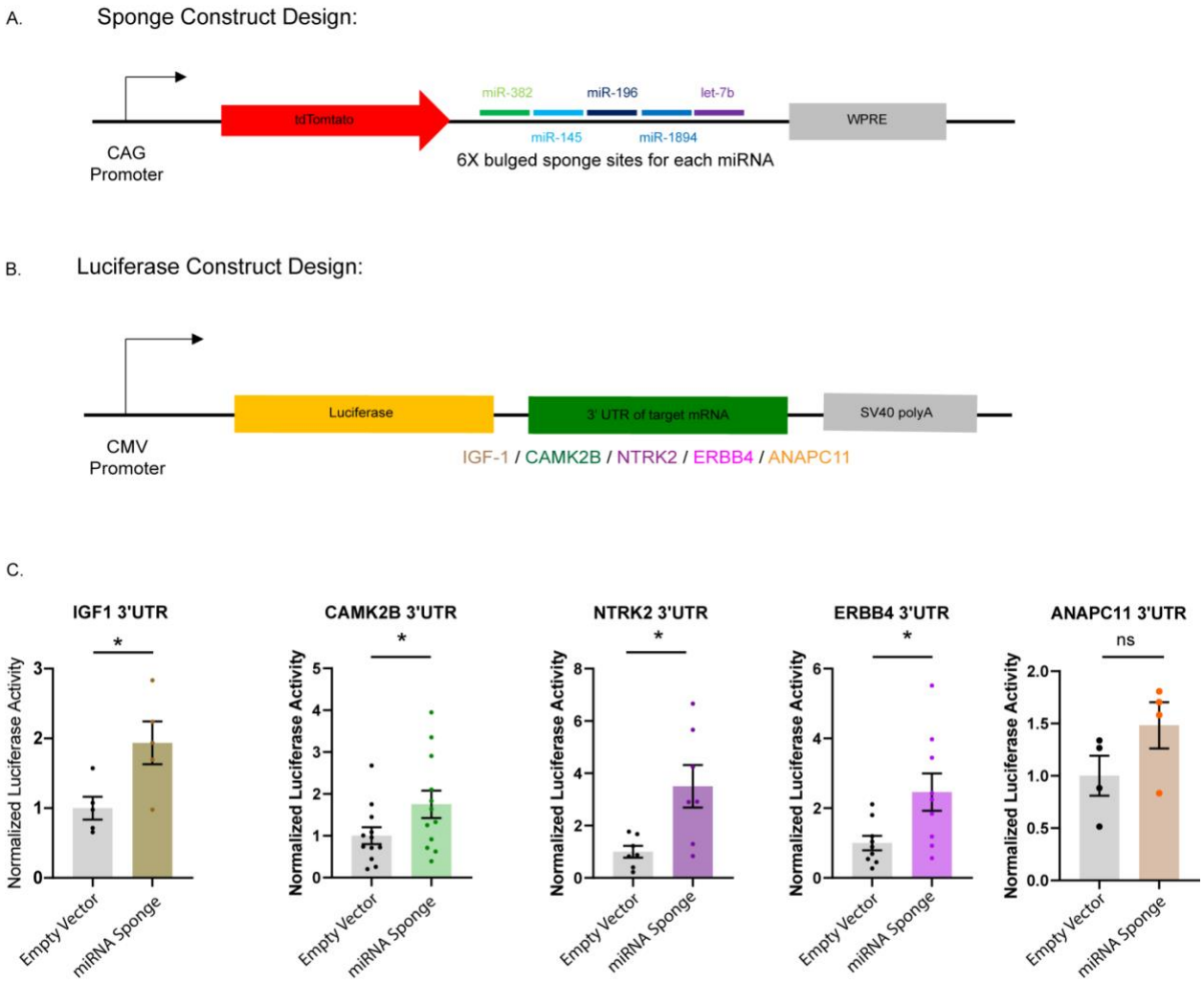

206

207

208 **Fig. 3: *In vitro* validation of mRNA target interactions with HFD responsive miRNAs**.

209 (A) Schematic design of miRNA sponge construct. (B) Schematic design of luciferase reporter. (C)
210 Quantitation of luciferase reporter expression driven by 3'UTRs of IGF1, NTRK2, CAMK2B, ERBB4
211 and ANAPC11 following simultaneous inhibition of all 5 HFD-regulated miRNAs' activity. N = 4 –
212 11 independent experiments. *$p < 0.05$. Data shown as mean ± SEM. Two tailed t-test with Welch's
213 correction.

214 **HFD-induced miRNAs specifically promote the generation of nascent AgRP$^+$ neurons.**

215 To determine the fate of adult born BrdU$^+$ nascent neurons upon HFD feeding, we have analyzed
216 whether these neurons differentiate into POMC-expressing anorexigenic or AgRP-expressing
217 orexigenic neurons in the MEm of the hypothalamus. Following HFD/NCD feeding, BrdU labelled
218 cells were analyzed for the co-expression of AgRP and POMC along with NeuN. HFD-fed mice
219 showed a significant enhancement of AgRP expressing BrdU$^+$ neurons (59.59% ± 19.88%
220 increase, $p = 0.004$) as compared to mice fed with NCD (Fig. 4A and Fig. 4B). We detected a similar
221 increase of POMC expressing BrdU$^+$ neurons (83.35% ± 27.33% increase, $p = 0.004$) in HFD-fed
222 mice (Fig. 4C – 4D). Next, we analyzed whether inhibition of the HFD-induced miRNAs could affect
223 the generation of AgRP$^+$ or POMC$^+$ neurons. A miRNA sponge against all the five HFD-upregulated
224 miRNAs was cloned into AAV-CAG-tdTomato and the AAV-tdTomato -miRNA sponge virus
225 injected into the hypothalamus of adult female mice. miRNA sponge expression was confirmed by
226 the expression of the tdTomato reporter (Fig. S1). The resultant inhibition of the HFD-induced
227 miRNAs reduced the number of AgRP$^+$ neurons (43.89% ± 2.915% decrease, $p < 0.0001$) (Fig. 5A
228 – 5B). In contrast, there was a minimal but statistically significant increase in POMC$^+$ neurons
229 (28.89% ± 3.376% increase, $p < 0.0001$) (Fig. 5C – 5D). Our observations reveal a surprising
230 insight: acute HFD-feeding paradigm selectively promotes the generation of AgRP+ orexigenic
231 neurons through a miRNA-dependent mechanism, while the generation of POMC+ anorexigenic
232 neurons remains unaffected by these miRNAs.

A.

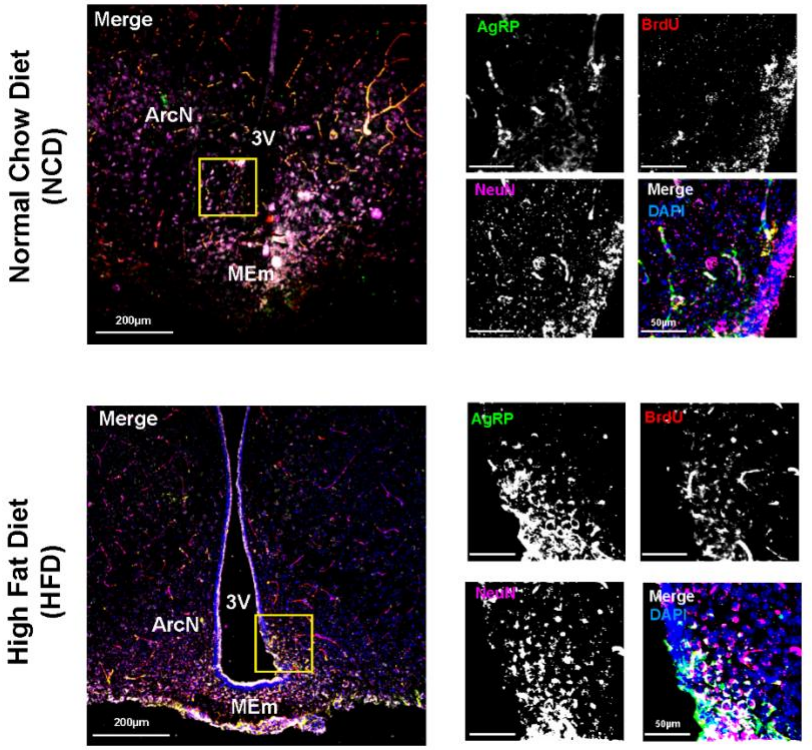
Normal Chow Diet (NCD)
High Fat Diet (HFD)
Merge
ArcN
3V
MEm
200µm
AgRP
BrdU
NeuN
Merge
DAPI
50µm

B.

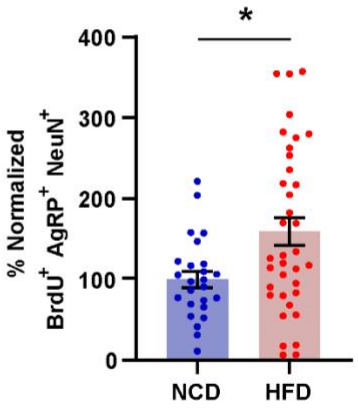
*
400
300
200
100
0
% Normalized
BrdU+ AgRP+ NeuN+
NCD
HFD

C.

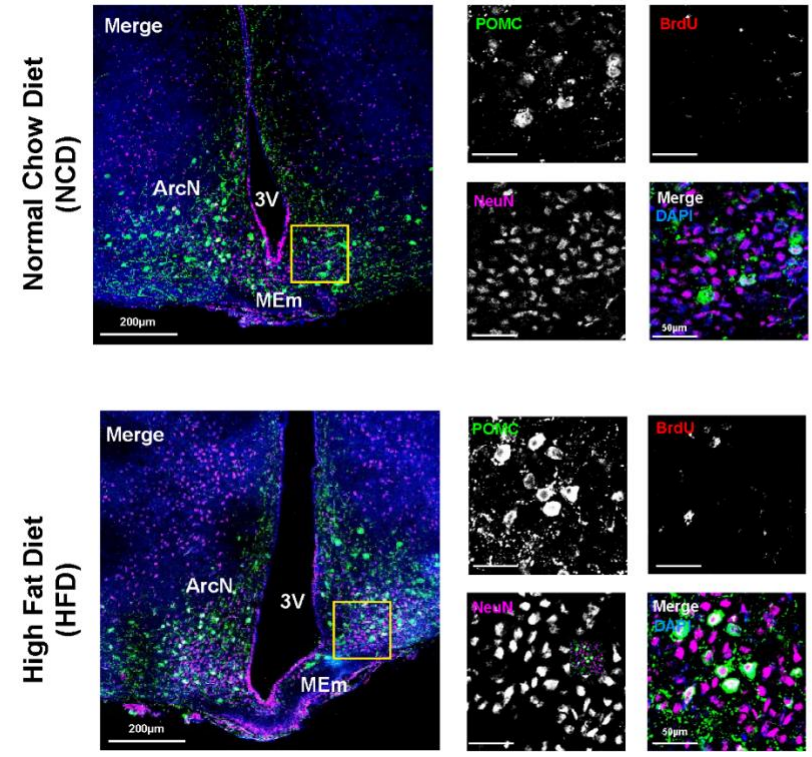
Normal Chow Diet (NCD)
High Fat Diet (HFD)
Merge
ArcN
3V
MEm
200µm
POMC
BrdU
NeuN
Merge
DAPI
50µm

D.

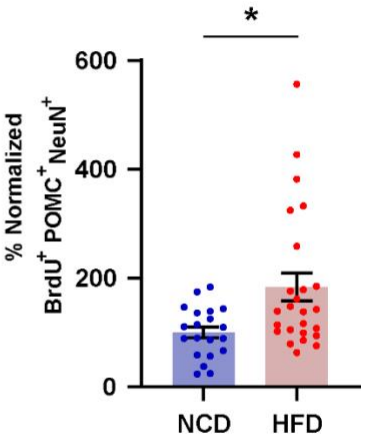
*
600
400
200
0
% Normalized
BrdU+ POMC+ NeuN+
NCD
HFD

233

234 **Fig. 4: Cell fate of tanycytic derived neurons in the hypothalamic feeding circuitry.**

235 (A) Photomicrographs represent orexigenic fate of diet-induced nascent neurons upon HFD or NCD
236 feeding. Low magnification image of brain section of all channels [DAPI (blue), BrdU (red), AgRP
237 (green), NeuN (magenta)] were merged (white). High magnification images of brain sections
238 labelled with DAPI (blue), BrdU (red), AgRP (green), NeuN (magenta) and merged (white). Scale
239 bars are as indicated. (B) Quantitative analysis of the number of colocalized $BrdU^+$ cells with $AgRP^+$
240 and $NeuN^+$ in the feeding circuit of mice after NCD and HFD feeding. n = 25-36 sections. N = 3
241 mice. *$p < 0.005$. Data shown as mean ± SEM. Two tailed t-test with Welch's correction. (C)
242 Photomicrographs represent anorexigenic fate of diet-induced nascent neurons upon HFD or NCD
243 feeding. Low magnification image of brain section of all channels [DAPI (blue), BrdU (red), POMC
244 (green), NeuN (magenta)] were merged (white). High magnification images of brain sections
245 labelled with DAPI (blue), BrdU (red), POMC (green), NeuN (magenta) and merged (white). Scale
246 bars are as indicated. (B) Quantitative analysis of the number of colocalized $BrdU^+$ cells with
247 $POMC^+$ and $NeuN^+$ in the feeding circuit of mice after NCD and HFD feeding. n = 20-25 sections.
248 N = 3 mice. *$p < 0.005$. Data shown as mean ± SEM. Two tailed t-test with Welch's correction.

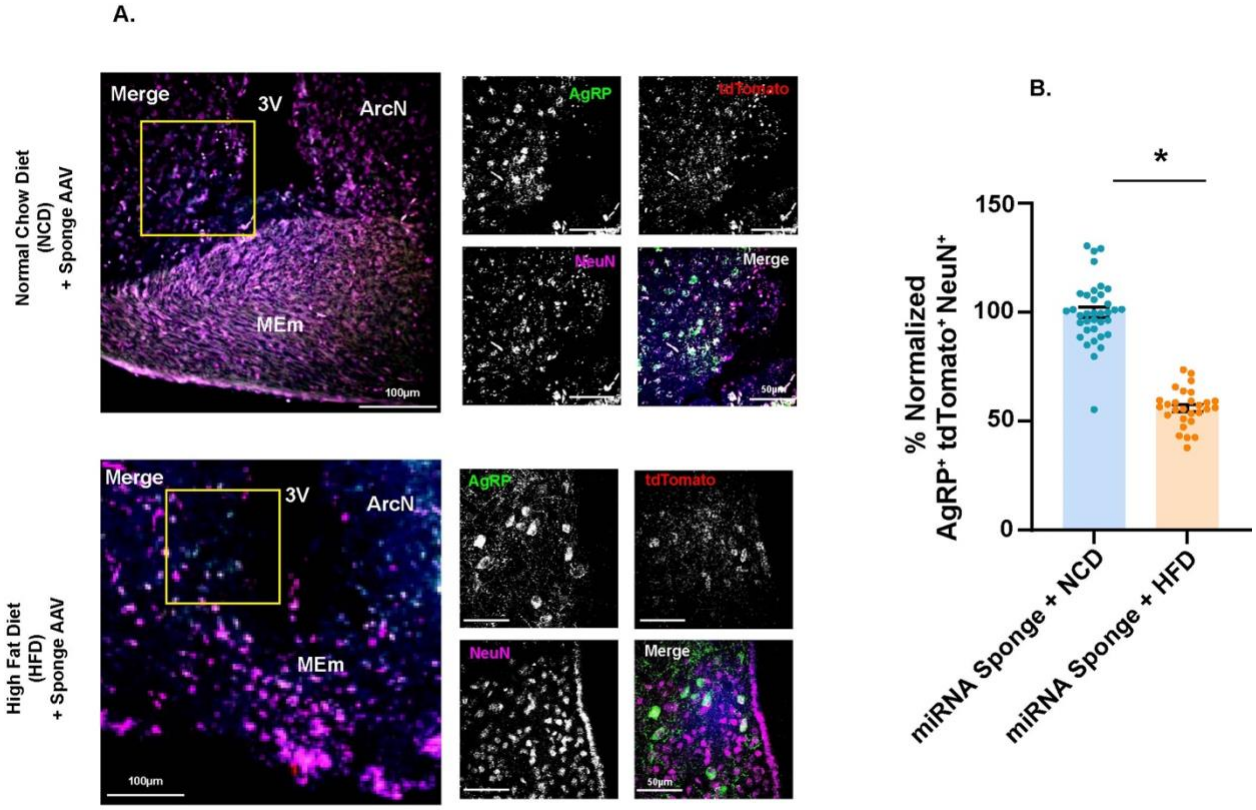
A.
Normal Chow Diet (NCD) + Sponge AAV
High Fat Diet (HFD) + Sponge AAV
Merge
3V
ArcN
MEm
AgRP
tdTomato
NeuN
100µm
50µm
B.
% Normalized AgRP+ tdTomato+ NeuN+
150
100
50
0
*
miRNA Sponge + NCD
miRNA Sponge + HFD

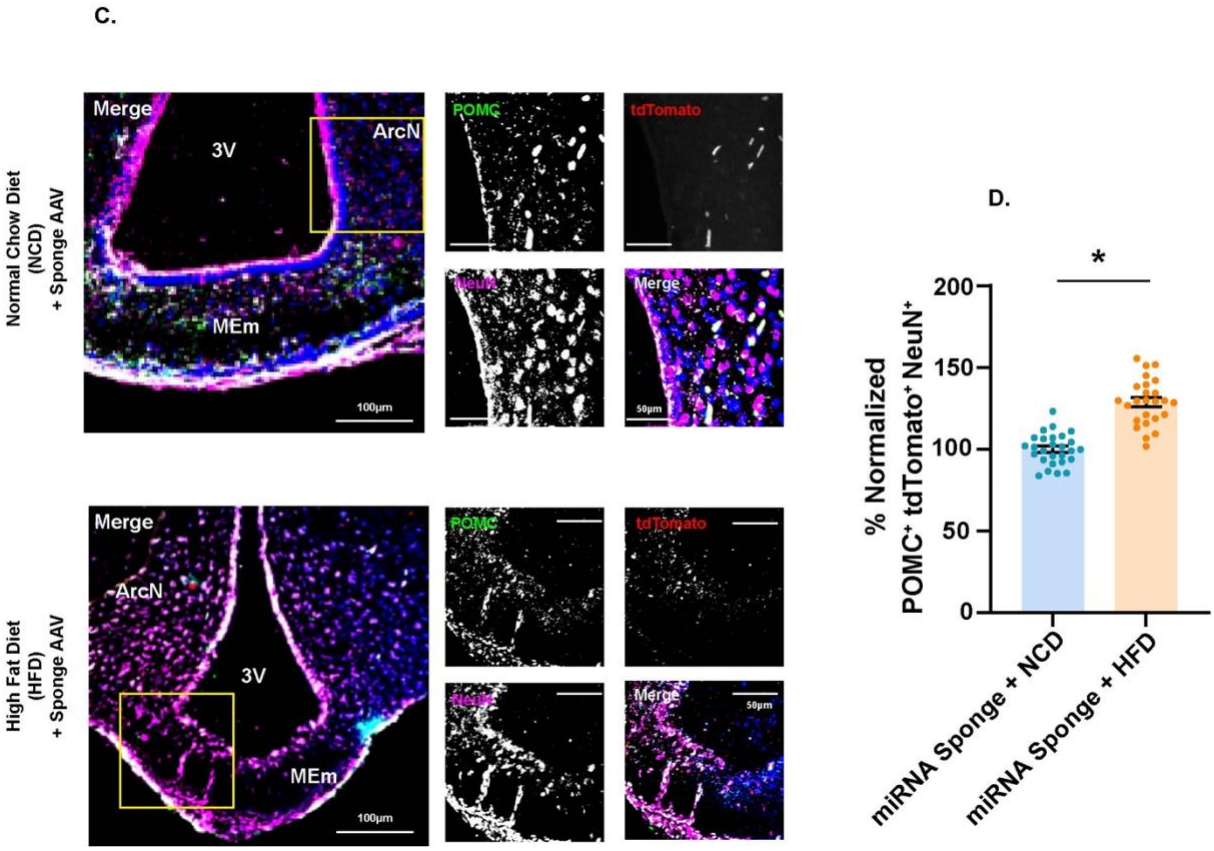
C.
Normal Chow Diet (NCD) + Sponge AAV
High Fat Diet (HFD) + Sponge AAV
Merge
3V
ArcN
MEm
POMC
tdTomato
NeuN
100µm
50µm
D.
% Normalized POMC+ tdTomato+ NeuN+
200
150
100
50
0
*
miRNA Sponge + NCD
miRNA Sponge + HFD

249

250 **Fig. 5: Inhibition of HFD –induced miRNAs prevents generation of orexigenic AgRP neurons.**

251 (A) Photomicrographs represent abrogation of orexigenic fate of the hypothalamic feeding circuit
252 upon HFD or NCD feeding. Low magnification image of brain section of all channels [DAPI (blue),
253 AAV –expressed tdTomato (red), AgRP (green), NeuN (magenta)] were merged (white). High
254 magnification images of brain sections labelled with DAPI (blue), tdTomato (red), AgRP (green),
255 NeuN (magenta) and merged (white). Scale bars are as indicated. (B) Quantitative analysis of the
256 number of colocalized $AgRP^+$ cells with $tdTomato^+$ and $NeuN^+$ in the feeding circuit of mice after
257 NCD and HFD feeding. n = 28-36 sections. N = 3 mice. *p < 0.0001. Data shown as mean ± SEM.
258 Two tailed t-test with Welch's correction. (C) Photomicrographs represent increase of anorexigenic
259 fate of the hypothalamic feeding circuit upon HFD or NCD feeding. Low magnification image of
260 brain section of all channels [DAPI (blue), AAV –expressed tdTomato (red), POMC (green), NeuN
261 (magenta)] were merged (white). High magnification images of brain sections labelled with DAPI
262 (blue), tdTomato (red), POMC (green), NeuN (magenta) and merged (white). Scale bars are as
263 indicated. (D) Quantitative analysis of the number of colocalized $POMC^+$ cells with $tdTomato^+$ and
264 $NeuN^+$ in the feeding circuit of mice after NCD and HFD feeding. n = 25-27 sections. N = 3 mice.
265 *p < 0.0001. Data shown as mean ± SEM. Two tailed t-test with Welch's correction.

266 **HFD-induced miRNAs promote the functional integration of newborn orexigenic $AgRP^+$**
267 **neurons**

268 We have quantified the number of $BrdU^+$ and c-Fos^+ neurons in the MEm and ArcN adjacent to
269 MEm as these areas contain mature POMC and AgRP neurons. AAVs containing either AAV-
270 tdTomato-miRNA sponge vector or control vector was injected into adult female mice and the
271 number of BrdU+ and c-Fos+ neurons were measured with or without the inhibition of HFD-induced
272 miRNAs. We observed a significant increase in $BrdU^+$ and c-Fos^+ neurons upon HFD feeding
273 (Table 1) (Fig. 6A - 6B) as compared to mice fed with NCD. The simultaneous inhibition of all HFD-
274 induced miRNAs resulted in a significant decrease in $BrdU^+$ and c-Fos^+ neurons (Table 1) (Fig. 6C
275 and 6D). Our data demonstrates that inhibition of HFD-induced miRNAs precludes the formation of
276 nascent neurons with functional properties.

277 We then examined the activity of orexigenic $AgRP^+$ and anorexigenic $POMC^+$ neurons by c-Fos
278 immunostaining after HFD feeding. HFD feeding promoted the activity of $AgRP^+$ (41.91% ± 3.801
279 % increase, p<0.0001), but not $POMC^+$ neurons (Fig. 7A – 7D).

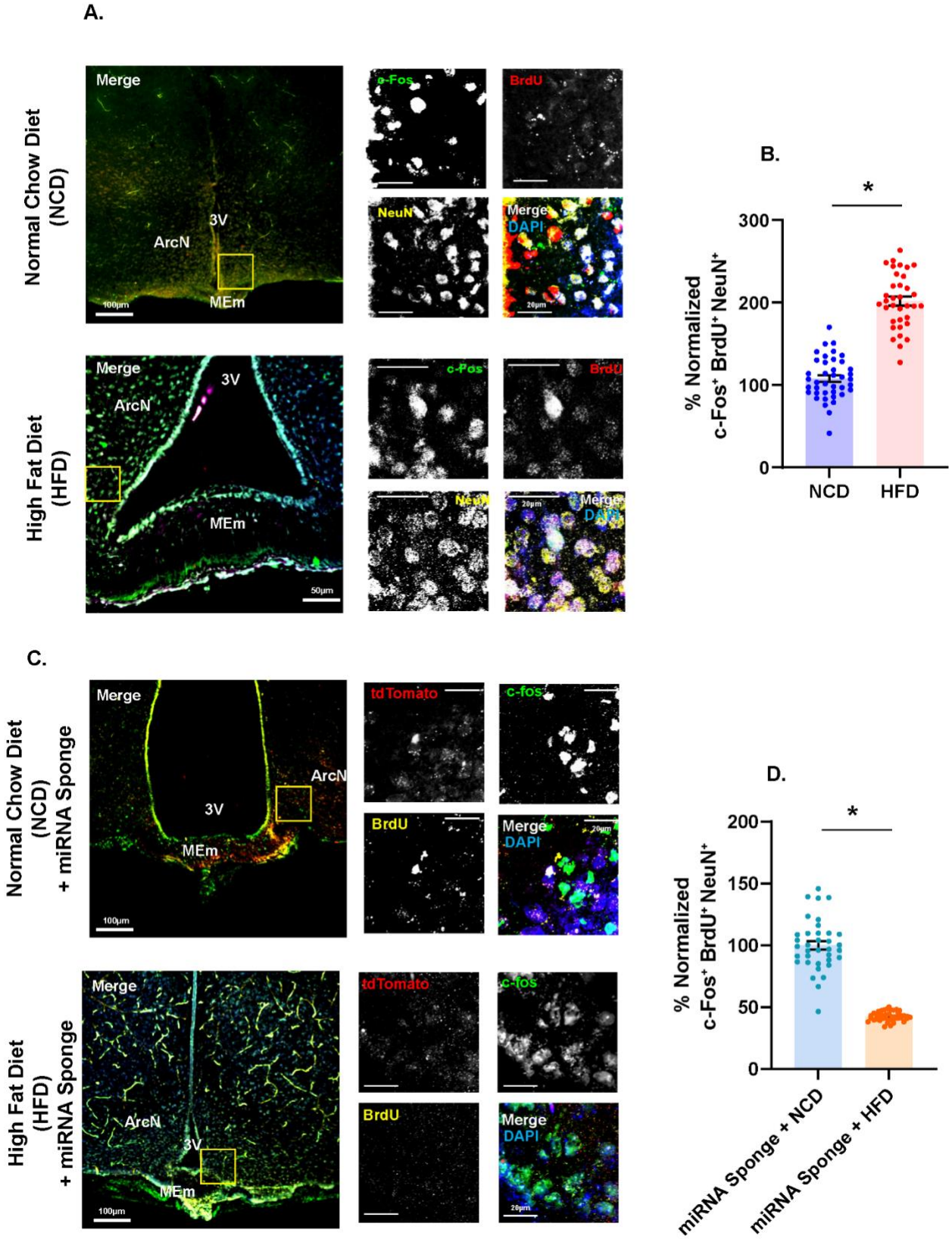
A.
Normal Chow Diet (NCD)
High Fat Diet (HFD)
Merge
c-Fos
BrdU
NeuN
DAPI
3V
ArcN
MEm
100µm
20µm
50µm
B.
% Normalized c-Fos⁺ BrdU⁺ NeuN⁺
300
200
100
0
NCD
HFD
*
C.
Normal Chow Diet (NCD) + miRNA Sponge
High Fat Diet (HFD) + miRNA Sponge
tdTomato
c-fos
D.
% Normalized c-Fos⁺ BrdU⁺ NeuN⁺
200
150
100
50
0
miRNA Sponge + NCD
miRNA Sponge + HFD

280

281 **Fig. 6: Inhibition of HFD -induced miRNAs block the activity of newborn neurons.**

282 (A) Photomicrographs represent functional activity of diet-induced nascent neurons in the
283 hypothalamic feeding circuitry upon HFD or NCD feeding. Low magnification image of brain
284 sections of all channels [DAPI (blue), BrdU (red), c-Fos (green), NeuN (yellow)] were merged
285 (white). High magnification images of brain sections labelled with DAPI (blue), BrdU (red), c-Fos
286 (green), NeuN (yellow) and merged (white). Scale bars are as indicated. (B) Quantitative analysis
287 of the number of colocalized $BrdU^+$ cells with $c\text{-}Fos^+$ and $NeuN^+$ in the feeding circuit of
288 hypothalamus after NCD and HFD feeding. n = 35-40 sections. N = 3 mice. *$p < 0.0001$. Data
289 shown as mean ± SEM. Two tailed t-test with Welch's correction. (C) Photomicrographs represent
290 abrogation of functional activity of diet-induced nascent neurons upon HFD or NCD feeding in the
291 hypothalamic feeding circuitry. Low magnification image of brain sections of all channels [DAPI
292 (blue), AAV –expressed tdTomato (red), c-Fos (green), NeuN (yellow)] were merged (white). High
293 magnification images of brain sections labelled with DAPI (blue), tdTomato (red), c-Fos (green),
294 BrdU (yellow) and merged (white). Scale bars are as indicated. (B) Quantitative analysis of the
295 number of colocalized $BrdU^+$ cells with $c\text{-}Fos^+$ and $tdTomato^+$ in the feeding circuit of mice after
296 NCD and HFD feeding. n = 36-41 sections. N = 3 mice. *$p < 0.0001$. Data shown as mean ± SEM.
297 Two tailed t-test with Welch's correction.

A.

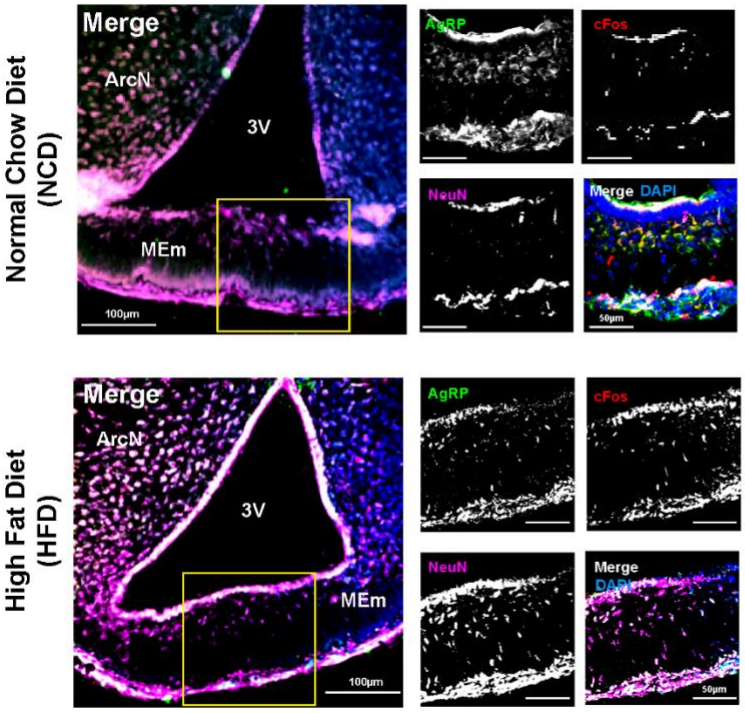
Normal Chow Diet (NCD)
High Fat Diet (HFD)
Merge
ArcN
3V
MEm
100µm
AgRP
cFos
NeuN
Merge DAPI
50µm

B.

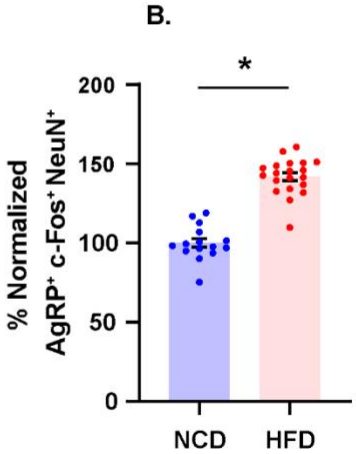
*
% Normalized AgRP⁺ c-Fos⁺ NeuN⁺
200
150
100
50
0
NCD
HFD

C.

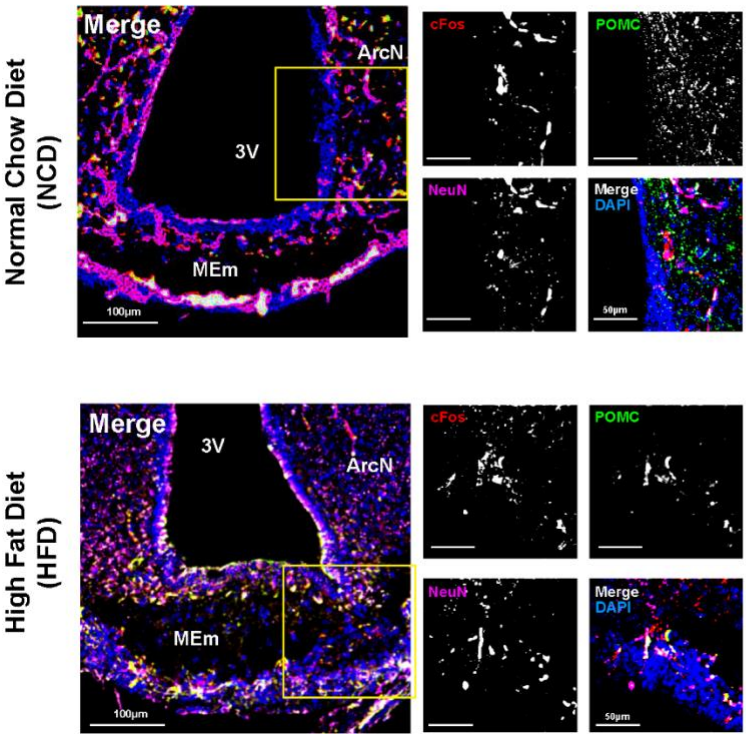
Normal Chow Diet (NCD)
High Fat Diet (HFD)
Merge
ArcN
3V
MEm
100µm
cFos
POMC
NeuN
Merge DAPI
50µm

D.

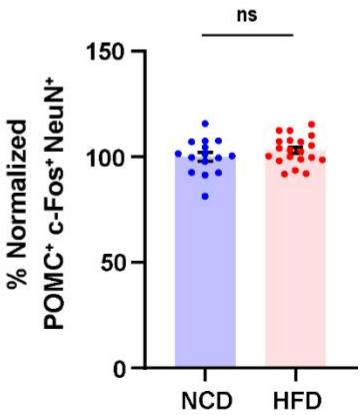
ns
% Normalized POMC⁺ c-Fos⁺ NeuN⁺
150
100
50
0
NCD
HFD

298

299 **Fig. 7: HFD administration enhances the activity of AgRP neurons in hypothalamus.**

300 (A) Photomicrographs represent abrogation of functional activity of orexigenic neurons in the
301 hypothalamic feeding circuitry upon HFD or NCD feeding. Low magnification image of brain
302 sections of all channels [DAPI (blue), c-Fos (red), AgRP (green), NeuN (magenta)] were merged
303 (white). High magnification images of brain sections labelled with DAPI (blue), c-Fos (red), AgRP
304 (green), NeuN (magenta) and merged (white). Scale bars are as indicated. (B) Quantitative analysis
305 of the number of colocalized $AgRP^+$ cells with c-Fos^+ and $NeuN^+$ in the feeding circuit of
306 hypothalamus after NCD and HFD feeding. n = 15-20 sections. N = 3 mice. *$p < 0.0001$. Data
307 shown as mean ± SEM. Two tailed t-test with Welch's correction. (C) Photomicrographs represent
308 functional activity of orexigenic neurons in the hypothalamic feeding circuitry upon HFD or NCD
309 feeding. Low magnification image of brain sections of all channels [DAPI (blue), c-Fos (red), POMC
310 (green), NeuN (magenta)] were merged (white). High magnification images of brain sections
311 labelled with DAPI (blue), c-Fos (red), POMC (green), NeuN (magenta) and merged (white). Scale
312 bars are as indicated. (D) Quantitative analysis of the number of colocalized $POMC^+$ cells with c-
313 Fos^+ and $NeuN^+$ in the feeding circuit of hypothalamus after NCD and HFD feeding. n = 15-20
314 sections. N = 3 mice. $p = 0.262$. Data shown as mean ± SEM. Two tailed t-test with Welch's
315 correction.

316 **Inhibition of HFD-induced miRNAs in hypothalamus prevents body weight gain and the**
317 **concomitant increase in liver fat mass.**

318 We wanted to investigate the physiological relevance of the HFD-feeding induced, miRNA-
319 dependent neurogenesis of orexigenic $AgRP^+$ neurons and their integration into the feeding
320 circuitry. Accordingly, we examined alterations in body weight and hepatic lipid accumulation
321 following the inhibition of diet -induced miRNAs in the presence of HFD**.** AAVs containing the AAV-
322 tdTomato-miRNA sponge vector or control vector was injected into the MEm and the ArcN
323 (adjacent to MEm) of female mice at P25, following which the mice were subjected to HFD / NCD
324 feeding paradigms during P45 - P75 and their body weight measured for the duration. HFD-feeding
325 resulted in enhanced body weight (Table 1) at P75. This gain was abrogated after inhibition of diet
326 -induced miRNAs (Fig. 8A – 8B) despite HFD-feeding. We further used MRI to determine the
327 accumulation of hepatic fat following the inhibition of HFD-induced miRNAs in the presence or
328 absence of HFD. HFD feeding led to enhanced fat mass in the liver (Table 1). The accumulation of
329 liver fat mass in female mice was abolished when HFD-induced miRNAs were inhibited (Fig. 8C –
330 8D).

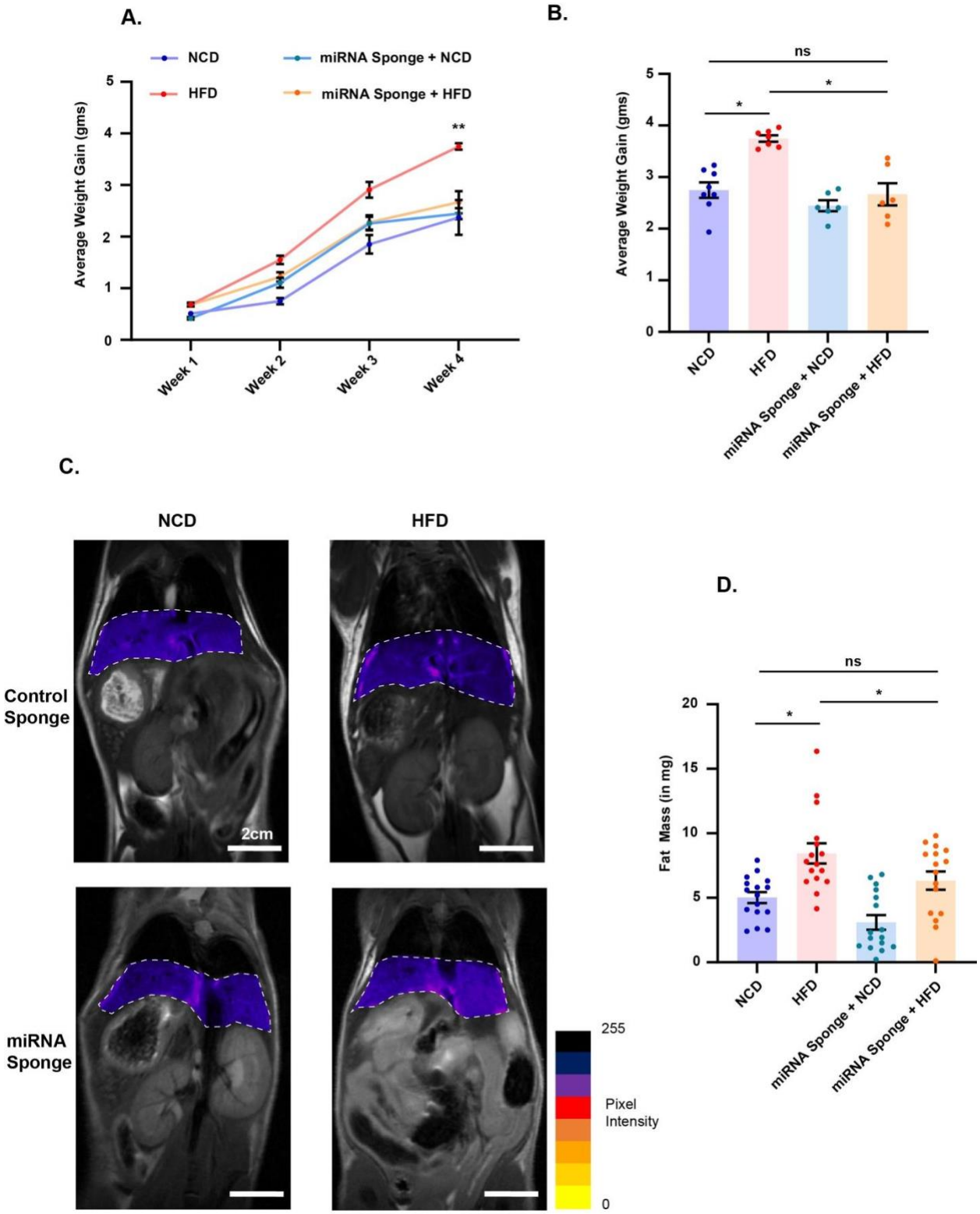
A.
NCD
HFD
miRNA Sponge + NCD
miRNA Sponge + HFD
Average Weight Gain (gms)
**
Week 1
Week 2
Week 3
Week 4
B.
ns
*
*
Average Weight Gain (gms)
NCD
HFD
miRNA Sponge + NCD
miRNA Sponge + HFD
C.
NCD
HFD
Control Sponge
miRNA Sponge
2cm
255
Pixel Intensity
0
D.
ns
*
*
Fat Mass (in mg)
NCD
HFD
miRNA Sponge + NCD
miRNA Sponge + HFD

331

332

333 **Fig. 8: HFD -induced body weight gain and hepatic fat accumulation is prevented by**
334 **inhibition of diet -regulated miRNAs.**

335 (A) Line plot of body weight gain measurements of mice fed with HFD or NCD, with or without the
336 injections of sponge, for the duration of the feeding. N = 3 mice. **p < 0.0032. Data shown as mean
337 ± SEM. Two tailed t-test with Welch's correction. (B) Average body weight gain of mice fed with
338 HFD or NCD, with or without the injections of sponge, at the end of the experiment (Weight at P75
339 – Weight at P45). N = 6-8 mice. *p < 0.0001. Data shown as mean ± SEM. Two tailed t-test with
340 Welch's correction. (C) Representative photomicrographs of T2- weighted MR Images of mice fed
341 with HFD or NCD, with or without the injections of sponge, at P75. The highlighted hepatic region
342 was selected for intensity analysis to determine fat mass in liver. (D) Quantification of hepatic fat
343 mass analyzed from MR Images of mice fed with HFD or NCD, with or without the injections of
344 sponge, at P75. n = 16 sections. N = 3 mice. *p < 0.0001. Data shown as mean ± SEM. Two tailed
345 t-test with Welch's correction.

346

347 **Discussion**
348

349 Recent studies highlight how diet-induced neurogenesis and neuronal plasticity in the
350 hypothalamus can profoundly influence feeding behaviour, energy expenditure, and systemic
351 metabolism (4, 5, 37). Emerging evidence indicates that adult neurogenesis is dynamically
352 regulated by both acute and chronic high-fat diet (HFD) exposure, contributing to divergent forms
353 of obesity with distinct metabolic phenotypes. Notably, acute HFD feeding paradigms result in
354 tanycytic neurogenesis from specific niches in the hypothalamus (5).

355 The current study attempts to reconcile physiological changes attributed to HFD exposure with
356 HFD-induced tanycytic neurogenesis in the hypothalamus. Here, we elucidate the molecular
357 underpinnings of neurogenesis from β2 tanycytes in the hypothalamus of young adult female mice
358 following acute HFD feeding. We have identified a cohort of miRNAs that are expressed from
359 different chromosomes, rather than a cluster of miRNAs from a single locus, after acute HFD
360 feeding (Fig. 1). Network analysis revealed their shared mRNA targets, with GO terms implicating
361 neurogenesis/differentiation regulators (Fig 2). A reporter assay confirmed the miRNA-mediated
362 regulation of key hub transcripts, such as IGF1, CAMK2B, NTRK2 and ERBB4 (Fig. 3). HFD-
363 induced miRNAs collectively favour the generation of functionally active (c-Fos+), orexigenic
364 AgRP+ neurons over the anorexigenic POMC+ neurons (Fig. 4 - 6). Interestingly, simultaneous
365 inhibition of all five HFD-induced miRNAs impaired the functional integration of newborn AgRP+
366 neurons into the hypothalamic feeding circuitry (Fig. 6 – 7); while also attenuating HFD-dependent
367 body weight gain and hepatic fat accumulation (Fig. 8).

368 Several studies underscore the role of miRNA-mediated regulation in the modulation of
369 hypothalamic feeding circuits with profound implications in obesity and metabolic control. Price *et*
370 *al.* (35) found that miR-33 deletion in AgRP+ neurons increases their activity, boosting food intake

371 and weight gain while causing metabolic dysregulation and worsening hepatic fat accumulation.
372 LaPierre *et al.* (36) showed that deletion of miR-7 (a miRNA highly expressed in the hypothalamus)
373 disrupts melanocortin signaling, promoting obesity. However, a holistic perspective on how diet-
374 modified miRNAs concertedly function to induce neurogenesis and modify the feeding circuitry is
375 unexplored (8, 38–41).

376 Our study resolves this void by identifying five HFD-induced miRNAs from β2 tanycytes in the MEm
377 of adult hypothalamus. Network analysis revealed a unique set of mRNA transcripts that are
378 combinatorially controlled by these five HFD-induced miRNAs; allowing us to inspect the regulatory
379 pathways associated with neurogenesis, neuronal differentiation and diet-induced metabolic
380 changes with greater resolution. These transcripts are positioned at key hubs within the network
381 that can influence many nodes. GO analysis of the target mRNAs confirmed the existence of a
382 neurogenic network that is regulated by HFD-induced miRNAs; with GO terms such as "response
383 to hormone", "neuron differentiation", "regulation of cell migration" etc. showing maximum
384 enrichment. Overall, a high degree of network modularity biased towards neurogenesis was
385 observed in the target mRNAs of HFD-induced miRNAs, which was notably absent in the targets
386 of NCD-induced miRNAs.

387 We developed an in-house miRNA sponge, which had complementary seed sequences against all
388 five HFD-induced miRNAs aligned in tandem. The miRNA sponge had a greater degree of affinity
389 to the miRNAs than their endogenous targets. Previous tanycyte ablation studies (5, 8) using X-ray
390 irradiation lacked molecular specificity as they completely eliminated tanycytes. Our miRNA-
391 sponge approach overcomes this limitation, revealing how specific miRNAs precisely regulate the
392 translational landscape of the β2-tanycytic neurogenic niche at a molecular resolution. Notably,
393 the development of a miRNA sponge serves as a proof-of-concept for RNA-based therapeutic
394 strategies aimed at preventing obesity.

395 Modification of a neuronal circuitry may be achieved by the functional integration of newborn
396 neurons into the pre-existing circuit; such neurons exhibit c-Fos expression (42). We found
397 progenitors from β2 tanycytes differentiate into both orexigenic $AgRP^+$ and anorexigenic $POMC^+$
398 neurons after HFD feeding. However, inhibiting HFD-induced miRNAs significantly reduced AgRP+
399 neurons but didn't affect POMC+ neuron generation, suggesting that HFD-induced miRNAs favour
400 orexigenic neurogenesis. Expression of c-Fos in nascent $AgRP^+$, but not $POMC^+$ neurons suggest
401 that these $POMC^+$ neurons are not functionally active. A plausible reason being that the life of
402 nascent $POMC^+$ neurons under acute HFD-feeding paradigms are transient in nature. We postulate
403 that β2 tanycyte-derived $POMC^+$ neurons may act as a "brake" to HFD-induced metabolic changes.
404 miRNAs upregulated under HFD favours the genesis and integration of orexigenic neurons into the

405 feeding circuitry to create a sustained physiological demand for high fat containing diet. Acute HFD
406 therefore fails to functionally integrate anorexigenic POMC neurons, favouring orexigenic-driven
407 hyperphagia and weight gain, as mentioned in previous studies (5, 11). This impairment of
408 functional POMC neuron integration is of potential therapeutic interest in countering the deleterious
409 effects of high-fat diets.

410 This study offers two potential avenues of therapeutic intervention; a) targeting the miRNAs that
411 are enriched by HFD using endogenously expressed miRNA sponges; b) overcoming molecular
412 paradigms that inhibit the integration of nascent POMC+ neurons.

413 Although miRNA-dependent mechanisms of HFD-induced tanycytic neurogenesis has been
414 characterized in young adult female mice, observations on further changes within tanycytic neurons
415 in older animals is beyond the scope of this study. Future investigations on age-dependent and
416 sex-dependent discrepancies in the molecular identities of HFD-induced newborn neurons may
417 provide useful insights towards combating metabolic disorders such as obesity and hyperphagia.

418 Collectively, the findings from our study reveal the molecular underpinnings of an unexplored
419 mechanism linking HFD-induced, miRNA-mediated neurogenesis in β2 tanycytes to weight gain
420 and hepatic fat accumulation, that is driven by the selective integration of AgRP+ neurons into the
421 feeding circuit.

422 Materials and Methods

423 Stereotaxic surgery for cannula implantation:

424 Female C57BL6/j animals at P21 - P25 were used for the experiments. Cannulas were prepared
425 from a 23G needle, modified for the appropriate ventral depth to be placed atop the skull as
426 described in (43). They were fitted with a dummy copper wire inside to prevent the leak of CSF or
427 the entry of external irritants into the lateral ventricle. This cannula structure was then sterilized
428 before the surgeries.
429 Animals were anaesthetized with Ketamine (80mg per 1 kg of body weight) and Xylazine (20mg
430 per 1kg of body weight) administered via subcutaneous injections. Post anaesthesia, the hairs were
431 trimmed, and the animals were affixed onto the stereotactic instrument. The skull was exposed and
432 the coordinates of the Bregma was determined. A hole for the cannula was drilled at the stereotaxic
433 coordinates (Anterior +0.02cm; Lateral -0.08cm; Ventral -0.25cm w.r.t Bregma). Stereotaxic
434 coordinates were obtained from the Mouse Coronal Atlas from the Allen Brain Atlas (mouse.brain-
435 map.org). The cannula was lowered at the previously drilled site. Post the implant of the cannula,
436 a small hole was drilled on the skull posterior to the cannula. A small screw was screwed onto the
437 skull. Then, the skull was covered up with the dental cements and quick solidifying polymer. Then,
438 the animals were allowed to recover from surgeries for 10-12 days, with regular changing of the

439 sterile dummy copper wire inside the cannula. Animal experiments were performed with the
440 approval of the Institutional Animal Ethics (IAEC) committee of National Brain Research Centre.

441 **Feeding and Intracerebroventricular/Intraperitoneal injections of BrdU:**

442 Animals were either started on a Rodent Diet with 60 kcal% fat diet (Research Diets, Inc. (RD
443 #12492)) [HFD], or continued with the normal chow diet [NCD] at P45, and this was continued till
444 they turned P75, when the animals were sacrificed for further experiments. Animals were given *ad*
445 *libitum* access to the diet and water. All the animals used for miRNA expression analysis via
446 TaqMan Arrays, were implanted with cannulas (n=3 animals for n=1 experiment for 3 experiments).
447 These animals were injected with BrdU intracerebroventricularly at 2 injections a day of 10 µgms
448 each from P45-P53. Mice used for immunostaining experiments were not implanted with cannulas
449 (n=1 animal for n=3 experiments). These animals were injected with 10mg of BrdU per kg body
450 weight intraperitoneally of the respective animals twice a day from P45-P53. Regular
451 measurements of body weights were noted from P45-P75.

452 **Immunostaining:**

453 Animals were anaesthetized and perfused transcardially at P75 with 1X PBS / 4%
454 Paraformaldehyde (PFA). The brains were then isolated and stored in PFA and processed with
455 30% Sucrose for cryosectioning. Brains were sectioned at 40 µm thickness and collected onto
456 gelatin-coated slides for processing. Sections were then introduced to an HCl and Borate Buffer
457 method for breaking the chromosomes and hybridized with anti-BrdU antibodies. They were also
458 co-stained with anti-Vimentin, anti-Nestin, anti-POMC, anti-AgRP, anti-c-Fos and anti-NeuN
459 antibodies as per the requirement of the different studies.

460 **Laser Capture Microscopy:**

461 Mice were anaesthetized and quickly perfused transcardially at P75 with 1X PBS on P75, and the
462 brains were isolated, and flash frozen in liquid N_2. Brains were sectioned at 12 µm thickness, and
463 carried onto MembraneSlide 1.0 PEN (Zeiss). Sections were fixed with PFA, then stained for BrdU
464 in RNase-free solutions, and conjugated with fluorescent tags to visualize under the microscope.
465 Zeiss PALM MicroBeam Laser Microdissection microscope was used to visualize the fluorescent
466 tags of BrdU. Manual ROIs were drawn around the fluorescent cells and they were micro dissected
467 with the MicroBeam laser. The cells were collected onto miRNA lysis buffers and pooled for miRNA
468 isolation using the Mirvana Total RNA isolation protocol (Applied Biosystems).

469 **TaqMan Low Density Array:**

470 The RNA from the captured neurogenic population was reverse transcribed using the Megaplex™
471 RT Primers, Rodent Pools Set v3.0. Then, the cDNA was amplified using Megaplex™ PreAmp
472 Primers, Rodent Pool Set v3.0. The amplified cDNA was then used to analyze the miRNA
473 expressions determined using TaqMan™ Array Rodent MicroRNA A+B Cards Set v3.0. Data was
474 then collected from 3 experiments, and average expression of the miRNAs were analyzed and
475 plotted.

476 **miRNA target identification:**

477 Annotated and putative targets of diet responsive miRNAs were obtained from the databases of
478 TargetScan (44), miRdb (45, 46) and PicTar (47). Common identified targets for each miRNA
479 across all the databases were acquired. Then, the common targets for the cohort of all diet
480 responsive miRNAs were also pooled into a single list of 1204 targets.

481 **Network Analysis:**

482 Interactions between the common targets of the HFD-enriched miRNAs were determined using the
483 String database (https://string-db.org/). The interaction network of the targets was then analyzed in
484 Matlab using Brain Connectivity Toolbox (24). All mRNA targets of the miRNAs were assigned as
485 nodes of the network and the interactions between two nodes were considered as the edges of the
486 network. Community analysis was performed using Louvain's method to determine the community
487 clusters of the nodes. Within module z-scores and participation coefficients were determined for
488 each node and plotted. Nodes were determined to be hubs if their corresponding z-scores were >
489 2.

490 **Gene Ontology Analysis:**

491 Hubs selected by z-score analysis were used for the analysis of Gene Ontologies using PANTHER
492 Database (http://pantherdb.org/) (doi:10.5281/zenodo.6399963). GO Enrichment for the hubs was
493 obtained from the database. Fisher's exact test was performed to test the significant enrichment of
494 the transcripts in annotated datasets such as, GO: Biological Process and Panther Pathways, and
495 the FDR values were generated using Panther statistical overrepresentation test. GO terms with
496 significant fold enrichment were analyzed and plotted.

497 **miRNA sponge construct design:**

498 Bulged binding sites against the seed sequences of HFD enriched miRNAs (from miRBase (48))
499 were designed and synthesized (49) 6 sites for each of the 5 miRNAs (miRs -382, -145, -196, -
500 1894 and let-7b) were included in the synthesized construct (50). This construct was then
501 incorporated into the ORF of the fluorescent marker tdTomato in Plasmid #59462 from Addgene.

502 An empty vector did not express the sponge sites. The plasmids were transfected into Neuro-2a
503 cells for luciferase assays, and they were packaged into AAVs for injection into the hypothalamus
504 for imaging. The designed sponge sequence is reported below with the bulged binding sites for
505 miR-382, miR-145, miR-196, miR-1894 and let-7b in the sequences.

506 miRNA Sponge Fwd. (5'–3')

507 AATTCAAAAAGTGCCACCGTGAATGATTATAAAAAGTGCCACCGTGAATGATTATAAAAAGTG
508 CCACCGTGAATGATTATAAAAAGTGCCACCGTGAATGATTATAAAAAGTGCCACCGTGAATG
509 ATTATAAAAAGTGCCACCGTGAATGATTATCAAGAACATGCTTCCAGGAATTTATCAAGAACA
510 TGCTTCCAGGAATTTATCAAGAACATGCTTCCAGGAATTTATCAAGAACATGCTTCCAGGAAT
511 TTATCAAGAACATGCTTCCAGGAATTTATCAAGAACATGCTTCCAGGAATTTATATCAGGTGA
512 CCGATGTCGTTGTTATATCAGGTGACCGATGTCGTTGTTATATCAGGTGACCGATGTCGTTG
513 TTATATCAGGTGACCGATGTCGTTGTTATATCAGGTGACCGATGTCGTTGTTATATCAGGTGA
514 CCGATGTCGTTGTTATCTCCCTTCGATTCTCCCTTGCTTATCTCCCTTCGATTCTCCCTTGCT
515 TATCTCCCTTCGATTCTCCCTTGCTTATCTCCCTTCGATTCTCCCTTGCTTATCTCCCTTCGAT
516 TCTCCCTTGCTTATCTCCCTTCGATTCTCCCTTGCTTATGGGAAGGCGTGGGTTGTATAGTTA
517 TGGGAAGGCGTGGGTTGTATAGTTATGGGAAGGCGTGGGTTGTATAGTTATGGGAAGGCGT
518 GGGTTGTATAGTTATGGGAAGGCGTGGGTTGTATAGTTATTTATGGGAAGGCGTGGGTTGTA
519 TAGA

520 miRNA Sponge Rev. (5'–3')

521 TCTATACAACCCACGCCTTCCCATAAATAACTATACAACCCACGCCTTCCCATAACTATACAA
522 CCCACGCCTTCCCATAACTATACAACCCACGCCTTCCCATAACTATACAACCCACGCCTTCC
523 CATAACTATACAACCCACGCCTTCCCATAAGCAAGGGAGAATCGAAGGGAGATAAGCAAGG
524 GAGAATCGAAGGGAGATAAGCAAGGGAGAATCGAAGGGAGATAAGCAAGGGAGAATCGAA
525 GGGAGATAAGCAAGGGAGAATCGAAGGGAGATAAGCAAGGGAGAATCGAAGGGAGATAAC
526 AACGACATCGGTCACCTGATATAACAACGACATCGGTCACCTGATATAACAACGACATCGGT
527 CACCTGATATAACAACGACATCGGTCACCTGATATAACAACGACATCGGTCACCTGATATAA
528 CAACGACATCGGTCACCTGATATAAATTCCTGGAAGCATGTTCTTGATAAATTCCTGGAAGCA
529 TGTTCTTGATAAATTCCTGGAAGCATGTTCTTGATAAATTCCTGGAAGCATGTTCTTGATAAAT
530 TCCTGGAAGCATGTTCTTGATAAATTCCTGGAAGCATGTTCTTGATAATCATTCACGGTGGCA
531 CTTTTTATAATCATTCACGGTGGCACTTTTTATAATCATTCACGGTGGCACTTTTTATAATCAT
532 TCACGGTGGCACTTTTTATAATCATTCACGGTGGCACTTTTTATAATCATTCACGGTGGCACT
533 TTTTGAATT

534

535

536 **Luciferase reporter construct design:**

537 Primers to amplify the 3'UTR sequences of miRNA targets, IGF1, NTRK2, CAMK2B, ERBB4 and
538 ANAPC11 were designed. The 3'UTRs were amplified from mouse brain RNA samples and were
539 incorporated into the pMIR-Report vector into the 3'UTR of the luciferase reporter.

540 IGF1_F TTAAACAGTTAAGCTAGGAAGTGCAGGAAACAAGACC

541 IGF1_R ATCCTTTATTAAGCTCATCTTAGGCTCCAGGCTTTCG

542 NTRK2_F TTAAACAGTTAAGCTAGGCATCTCCCGTCTACCTG

543 NTRK2_R ATCCTTTATTAAGCTAGAGCGTCTCCTGTCTTTGTC

544 CAMK2B_F TTAAACAGTTAAGCTACGGCAAGTGGCAGAATGTAC

545 CAMK2B_R ATCCTTTATTAAGCTACCTGCATTGCCCAGAAGTC

546 ERBB4_F TTAAACAGTTAAGCTCGCCCTACAGACACCGGAATAC

547 ERBB4_R ATCCTTTATTAAGCTCCTTTCATGTAGACGTACCCAATCC

548 ANAPC11_F TTAAACAGTTAAGCTATGTGTCGCCAGGAGTGGAAG

549 ANAPC11_R ATCCTTTATTAAGCTAGTCTCCCAGAAGCACAAGTC

550 **Luciferase reporter assays:**

551 Neuro-2a cells were transduced with miRNA sponge, or control plasmid at 16 hrs post plating.
552 Transfected cells were incubated in high glucose DMEM media (Gibco) with 5% fetal bovine serum
553 and maintained at 5% CO_2 and 37°C. Cells were simultaneously co-transfected with Gaussia
554 luciferase containing the 3′UTRs of IGF1/ NTRK2/ CAMK2B/ ERBB4/ ANAPC11 and Firefly
555 luciferase cloned in pMIR-Report plasmid as well as pRLTK. Luciferase activities were measured
556 48 hrs post transfection. Dual Luciferase Reporter Assay System (Promega) was used to measure
557 the intensities of Gaussia and Firefly luciferases. Data was analyzed as the ratio of intensities from
558 Gaussia luciferase to Firefly luciferase.

559 **AAV Preparation and Stereotaxic Injection into arcuate nucleus:**

560 Adenovirus was produced by cotransfection of 9.55 µgm of empty plasmid (expressing tdTomato
561 by CAG promoter, #59462 from Addgene) or sponge plasmid (tdTomato with the sponge sequence

562 inserted in the ORF under the CAG promoter), 9.55 µgm pAAV2/9n and 19.22 µgm pAdDeltaF6 in
563 HEK293T cells. Calcium phosphate method of transfection was used to deliver the plasmids to
564 HEK293T cells. Cells were incubated in low glucose DMEM media (Gibco) with 10% fetal bovine
565 serum and maintained at 5% CO_2 and 37°C. 72 hours after transfection, media was collected, and
566 the cells were lysed and filtered with a 100-micron filter mesh. The media and lysed cells were
567 pooled, and viral pellets were obtained using ultracentrifugation. Viral particles were resuspended
568 in 1X PBS with 5% Glycerol.

569 Stereotaxic surgeries were performed on the mice aged P21-P25 to deliver the AAV containing
570 miRNA sponge to the arcuate nucleus as mentioned above. Using a Hamilton syringe, 200nL of
571 the AAVs were injected into the arcuate nucleus at the stereotaxic coordinates (Anterior -0.02 cm;
572 Lateral -0.002 cm; Ventral -0.059 cm; w.r.t Bregma). After the surgery, animals were allowed to
573 recover for 10-12 days before the feeding and injections were started.

574 **Confocal Imaging and Image Analysis:**

575 Brain sections stained and mounted were imaged using a Nikon A1 HD25 point scanning
576 microscope with a Nikon 20X Objective at a 1024*1024 resolution of pixels. Optical sections of 1µm
577 step sizes were captured for the entire brain sections. All captured images were of 16-bit pixel
578 depth, and had uniform laser power, detector gain and pinhole diameter values.

579 TIFFs of raw images were selected from all channels expressing DAPI, BrdU, POMC, AgRP, c-Fos
580 and NeuN. Using custom written MATLAB algorithms, all images were thresholded dynamically
581 with their respective background noise. Thresholded images at the same optical section depths
582 were used to quantify the underlying number of cells expressing in each channel as well as the
583 number of colocalization between the channels. The data was then exported, pooled, analyzed and
584 plotted for significance.

585 **miRNA Sponge Efficacy Analysis:**

586 Primary neuronal cultures were prepared from dissected mouse embryonic (E17) cortices as
587 described previously (51). About 160 to 170 cells/mm^2 were plated for verifying the efficacy of
588 miRNA sponge expression. Neurons were grown *in vitro* in Neurobasal medium (Gibco) containing
589 B27 supplements (Gibco) at 5% CO_2/37°C. Adenoviruses expressing miRNA sponge or empty
590 sponge vectors were transduced at DIV (days *in vitro*) 7. Neurons were fixed with 4%
591 paraformaldehyde at DIV 21 and were counterstained with DAPI containing media.

592 Neurons were imaged using a Nikon A1 HD25 point scanning microscope with a Nikon 100X
593 Objective at a 1024*1024 resolution of pixels. Optical sections of 0.2 µm step sizes were captured

594 for the entire neuron. All captured images were of 16-bit pixel depth, and had uniform laser power,
595 detector gain and pinhole diameter values.

596 Maximum Intensity Projections of each neuron were made as TIFFs from raw images and the
597 average global pixel intensities of tdTomato fluorescence were computed using Matlab. The data
598 was collected and pooled for statistical analysis.

599 **Magnetic Resonance Imaging and Analysis**

600 All imaging procedures were conducted using a 7.0 T Bruker BioSpec 70/20 USR AV3HD small-
601 animal MRI system (M/s Bruker BioSpin, Ettlingen, Germany), with Maximum gradient strength of
602 440 mT/m. A 70 mm quadrature volume coil was employed for both radiofrequency transmission
603 and reception.

604 Preparation: Mice at P75 were anaesthetized with Ketamine (80mg per 1 kg of body weight) and
605 Xylazine (20mg per 1kg of body weight) administered via subcutaneous injections. The animals
606 were positioned in a prone orientation (head-first in the scanner) with the abdomen centered within
607 the coil. Core body temperature was maintained at 36–37°C utilizing a warm-air feedback system,
608 and respiration was monitored via a pneumatic pillow sensor. Prospective respiratory gating was
609 applied to all sequences, with acquisitions triggered during end-expiration.

610 Imaging protocol: A respiratory-gated, two-dimensional T_2-weighted TurboRARE sequence
611 (Bruker: RARE) was utilized, with repetition times (TR) ranging from 1411-1852ms and an echo
612 time (TE) of 27ms. The echo train length (RARE factor) was conFig.d to 8, with a flip angle of 90°.
613 Images were acquired using a 320 × 320 reconstructed matrix, a 100% phase field of view, and an
614 in-plane resolution of approximately 0.10–0.125 mm, adjusted according to the field of view for
615 each subject. Both slice thickness and interslice spacing were set to 1.0 mm, with 8 signal averages
616 (NEX) and a pixel bandwidth of 244 Hz/pixel. The phase-encoding direction was designated as
617 either ROW or COL, contingent on anatomical geometry, to minimize motion ghosting. All
618 acquisitions employed prospective respiratory gating, triggered at end-expiration, and were
619 conducted in ParaVision Acquisition 6.0.1. For fat-suppressed acquisitions, the same sequence
620 geometry and parameters were maintained, with the addition of spectral fat-suppression applied at
621 the lipid resonance frequency prior to excitation to selectively attenuate the fat signal. Each gated
622 acquisition lasted approximately 3–6 minutes, depending on the respiratory rate.

623 Imaging Analysis: Raw Bruker data were converted to NIfTI format using dcm2niix
624 (v1.0.20240202), ensuring complete preservation of orientation metadata. Intensity histograms
625 were calculated from NIFTI format images. Using custom program in Matlab, Otsu's threshold was
626 applied to the images and voxels with high intensities (> Image Threshold) were considered as "fat

627 voxels" and intermediate intensities were considered as "lean voxels". Liver masks were generated
628 by manual ROIs to isolate hepatic fat from visceral fat. Voxel volumes were determined, and fat
629 mass was calculated with known density for fat tissue (0.9 gm/cm^3).

630 **Statistics**:

631 Statistical analysis was performed for all experiments. miRNA differential expressions were
632 analyzed for significance using two-tailed students' t-test and post hoc determination of false
633 discovery rates using the Benjamini-Hochberg method (52). Luciferase reporter assays and
634 intensity analysis for miRNA sponge expression were analyzed for significance using unpaired two-
635 tailed t-test with Welch's correction. Unpaired t-test with Welch's correction was used to determine
636 the significance for all immunostaining experiments including determination of orexigenic and
637 anorexigenic fate and their functional integration in the hypothalamic feeding neural circuit. The
638 functional activity of neurogenic cells was also analysed by unpaired t-test with Welch's correction.

639 **Acknowledgments**
640
641 We thank Addgene for AAV vectors. We thank Ananya Ghosh and Santhosh Kumar for the
642 technical assistance. This study was funded by the Department of Biotechnology, Government of
643 India (BT/PR8793/AGR/36/749/2013) and NBRC core fund to Sourav Banerjee.

644

645 **References**

646 1. J. Song, K. M. Christian, G. L. Ming, H. Song, Modification of hippocampal circuitry by adult
647 neurogenesis. *Dev. Neurobiol.* **72**, 1032–1043 (2012).

648 2. D. Lim, A. Alvarez-Buylla, The Adult Ventricular – Subventricular Zone and Olfactory bulb
649 Neurogenesis. *Cold Spring Harb. Perspect. Biol.* **8**, a018820 (2016).

650 3. S. Yoo, S. Blackshaw, Regulation and function of neurogenesis in the adult mammalian
651 hypothalamus. *Prog. Neurobiol.* (2018).

652 4. M. V. Kokoeva, H. Yin, J. S. Flier, Evidence for constitutive neural cell proliferation in the
653 adult murine hypothalamus. *J. Comp. Neurol.* **505** (2007).

654 5. D. A. Lee, *et al.*, Tanycytes of the hypothalamic median eminence form a diet-responsive
655 neurogenic niche. *Nat. Neurosci.* **15** (2012).

656 6. P. J. Enriori, *et al.*, Diet-Induced Obesity Causes Severe but Reversible Leptin Resistance
657 in Arcuate Melanocortin Neurons. *Cell Metab.* **5** (2007).

658 7. D. I. Briggs, *et al.*, Calorie-restricted weight loss reverses high-fat diet-induced ghrelin
659 resistance, which contributes to rebound weight gain in a ghrelin-dependent manner.
660 *Endocrinology* **154** (2013).

661 8. D. A. Lee, *et al.*, Dietary and sex-specific factors regulate hypothalamic neurogenesis in
662 young adult mice. *Front. Neurosci.* (2014). https://doi.org/10.3389/fnins.2014.00157.

663 9. T. C. Mathew, Regional analysis of the ependyma of the third ventricle of rat by light and
664 electron microscopy. *J. Vet. Med. Ser. C Anat. Histol. Embryol.* **37** (2008).

665 10. M. A. Cowley, *et al.*, Leptin activates anorexigenic POMC neurons through a neural network
666 in the arcuate nucleus. *Nature* **411** (2001).

667 11. Y. Aponte, D. Atasoy, S. M. Sternson, AGRP neurons are sufficient to orchestrate feeding
668 behavior rapidly and without training. *Nat. Neurosci.* **14** (2011).

669 12. J. W. Sohn, Network of hypothalamic neurons that control appetite. *BMB Rep.* (2015).

670 13. M. Bolborea, N. Dale, Hypothalamic tanycytes: potential roles in the control of feeding and
671 energy balance. *Trends Neurosci.* **36**, 91–100 (2013).

672 14. R. Dali, J. Estrada-Meza, F. Langlet, Tanycyte, the neuron whisperer. *Physiol. Behav.* **263**,
673 114108 (2023).

674 15. S. Sangiao-Alvarellos, L. Pena-Bello, M. Manfredi-Lozano, M. Tena-Sempere, F. Cordido,
675 Perturbation of Hypothalamic MicroRNA Expression Patterns in Male Rats After Metabolic
676 Distress: Impact of Obesity and Conditions of Negative Energy Balance. *Endocrinology* **155**,
677 1838–1850 (2014).

678 16. I. A. Vinnikov, *et al.*, Hypothalamic miR-103 Protects from Hyperphagic Obesity in Mice. *J.*
679 *Neurosci.* **34**, 10659–10674 (2014).

680 17. M. A. Lopez-Ramirez, S. Nicoli, Role of miRNAs and epigenetics in neural stem cell fate
681 determination. *Epigenetics* **9**, 90–100 (2014).

682 18. L. Stappert, F. Klaus, O. Brüstle, MicroRNAs Engage in Complex Circuits Regulating Adult
683 Neurogenesis. *Front. Neurosci.* **12** (2018).

684 19. X. Tang, G. Tang, S. Özcan, Role of microRNAs in diabetes. *Biochim. Biophys. Acta - Gene*
685 *Regul. Mech.* (2008).

686 20. P. Bielefeld, *et al.*, A standardized protocol for stereotaxic intrahippocampal administration
687 of kainic acid combined with electroencephalographic seizure monitoring in mice. *Front.*
688 *Neurosci.* **11** (2017).

689 21. J. G. Maldonado-Avilés, D. J. Guarnieri, X. Zhu, R. J. DiLeone, Down-regulation of miRNAs
690 in the brain and development of diet-induced obesity. *Int. J. Dev. Neurosci.* **64** (2018).

691 22. F. Zhang, *et al.*, Obesity-induced overexpression of miR-802 impairs insulin transcription
692 and secretion. *Nat. Commun.* **11** (2020).

693 23. M. Porniece Kumar, *et al.*, Insulin signalling in tanycytes gates hypothalamic insulin uptake
694 and regulation of AgRP neuron activity. *Nat. Metab.* **3** (2021).

695 24. M. Rubinov, O. Sporns, Complex network measures of brain connectivity: Uses and
696 interpretations. *Neuroimage* **52**, 1059–1069 (2010).

697 25. M. A. I. Åberg, N. D. Åberg, H. Hedbäcker, J. Oscarsson, P. S. Eriksson, Peripheral Infusion
698 of IGF-I Selectively Induces Neurogenesis in the Adult Rat Hippocampus. *J. Neurosci.* **20**,
699 2896–2903 (2000).

700 26. G. J. F. Brooker, *et al.*, Endogenous IGF-1 regulates the neuronal differentiation of adult
701 stem cells. *J. Neurosci. Res.* **59**, 332–341 (2000).

702 27. D. Aberg, Role of the growth hormone/insulin-like growth factor 1 axis in neurogenesis.
703 *Endocr. Dev.* (2009).

704 28. B. Xu, *et al.*, Brain-derived neurotrophic factor regulates energy balance downstream of
705 melanocortin-4 receptor. *Nat. Neurosci.* **6** (2003).

706 29. J. Gray, *et al.*, Functional characterization of human NTRK2 mutations identified in patients
707 with severe early-onset obesity. *Int. J. Obes.* **31** (2007).

708 30. F. F. Hamdan, *et al.*, High Rate of Recurrent De Novo Mutations in Developmental and
709 Epileptic Encephalopathies. *Am. J. Hum. Genet.* **101** (2017).

710 31. K. A. Miller, *et al.*, Diagnostic value of exome and whole genome sequencing in
711 craniosynostosis. *J. Med. Genet.* **54** (2017).

712 32. A. J. Rose, B. Kiens, E. A. Richter, Ca2+-calmodulin-dependent protein kinase expression
713 and signalling in skeletal muscle during exercise. *J. Physiol.* **574** (2006).

714 33. R. A. G. Garcia, K. Vasudevan, A. Buonanno, The neuregulin receptor ErbB-4 interacts with
715 PDZ-containing proteins at neuronal synapses. *Proc. Natl. Acad. Sci. U. S. A.* **97** (2000).

716 34. Y. Z. Huang, *et al.*, Regulation of neuregulin signaling by PSD-95 interacting with ErbB4 at
717 CNS synapses. *Neuron* **26** (2000).

718 35. N. L. Price, *et al.*, microRNA-33 controls hunger signaling in hypothalamic AgRP neurons.
719 *Nat. Commun.* **15**, 2131 (2024).

720 36. M. P. LaPierre, K. Lawler, S. Godbersen, I. S. Farooqi, M. Stoffel, MicroRNA-7 regulates
721 melanocortin circuits involved in mammalian energy homeostasis. *Nat. Commun.* **13**, 5733
722 (2022).

723 37. M. V. Kokoeva, H. Yin, J. S. Flier, Neurogenesis in the hypothalamus of adult mice: Potential
724 role in energy balance. *Science (80-.).* **310** (2005).

725 38. M. Schneeberger, A. G. Gomez-ValadÃ©s, S. Ramirez, R. Gomis, M. Claret, Hypothalamic
726 miRNAs: emerging roles in energy balance control. *Front. Neurosci.* **9** (2015).

727 39. C. Esau, *et al.*, miR-122 regulation of lipid metabolism revealed by in vivo antisense
728 targeting. *Cell Metab.* **3** (2006).

729 40. F. Olivieri, *et al.*, Hormone replacement therapy enhances IGF-1 signaling in skeletal
730 muscle by diminishing miR-182 and miR-223 expressions: A study on postmenopausal
731 monozygotic twin pairs. *Aging Cell* **13** (2014).

732 41. L. Jean-François, A. Derghal, L. Mounien, Micrornas in obesity and related metabolic
733 disorders. *Cells* **8** (2019).

734 42. S. Jessberger, G. Kempermann, Adult-born hippocampal neurons mature into activity-
735 dependent responsiveness. *Eur. J. Neurosci.* **18** (2003).

736 43. D. M. Kokare, G. P. Shelkar, C. D. Borkar, K. T. Nakhate, N. K. Subhedar, A simple and
737 inexpensive method to fabricate a cannula system for intracranial injections in rats and mice.
738 *J. Pharmacol. Toxicol. Methods* **64**, 246–250 (2011).

739 44. V. Agarwal, G. W. Bell, J.-W. Nam, D. P. Bartel, Predicting effective microRNA target sites
740 in mammalian mRNAs. *Elife* **4** (2015).

741 45. W. Liu, X. Wang, Prediction of functional microRNA targets by integrative modeling of
742 microRNA binding and target expression data. *Genome Biol.* **20**, 1–10 (2019).

743 46. Y. Chen, X. Wang, MiRDB: An online database for prediction of functional microRNA
744 targets. *Nucleic Acids Res.* **48**, D127–D131 (2020).

745 47. A. Krek, *et al.*, Combinatorial microRNA target predictions. *Nat. Genet.* **37**, 495–500 (2005).

746 48. A. Kozomara, M. Birgaoanu, S. Griffiths-Jones, MiRBase: From microRNA sequences to
747 function. *Nucleic Acids Res.* **47**, D155–D162 (2019).

748 49. M. S. Ebert, J. R. Neilson, P. A. Sharp, MicroRNA sponges: Competitive inhibitors of small
749 RNAs in mammalian cells. *Nat. Methods* **4** (2007).

750 50. J. Kluiver, *et al.*, Generation of miRNA sponge constructs. *Methods* **58** (2012).

751 51. S. Kaech, G. Banker, Culturing hippocampal neurons. *Nat. Protoc.* **1**, 2406–2415 (2006).

752 52. Y. Benjamini, Y. Hochberg, Controlling the False Discovery Rate: A Practical and Powerful
753 Approach to Multiple Testing. *J. R. Stat. Soc. Ser. B* **57**, 289–300 (1995).

754

Supporting Information for

High fat diet promotes obesity by driving miRNA dependent neurogenesis and integration of orexigenic neurons in the feeding circuitry

Balakumar Srinivasan[1], Sarbani Samaddar[1], Himanshu Singh[3], Senthil Kumaran[3], Dipanjan Roy[1, 2], and Sourav Banerjee[1]

1. National Brain Research Centre, NH8, Nainwal Mode, Manesar 122052, Haryana, INDIA
2. Current address: School of Artificial Intelligence and Data Science, Indian Institute of Technology, Jodhpur 342030, Rajasthan, INDIA
3. Department of NMR and MRI Facility, All India Institute of Medical Sciences, Ansari Nagar, New Delhi 110029, INDIA

Corresponding Author: Sourav Banerjee
Correspondence: souravnbrc@gmail.com or sourav@nbrc.ac.in

Figures

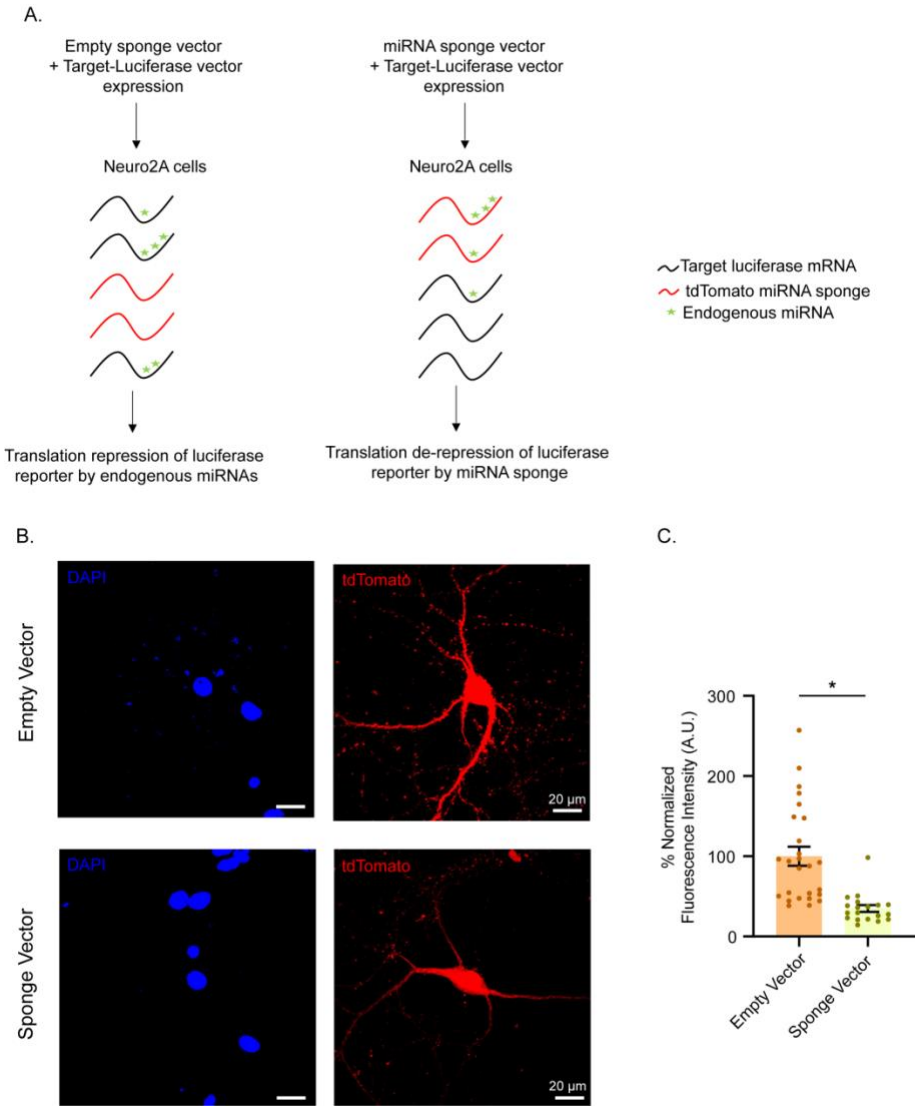

Fig S1: Inhibition of diet -regulated miRNAs by sponge

(A) Schematic for miRNA sponge-mediated inhibition of miRNA-mRNA target interaction as measured by reporter assay. (B). Photomicrograph representing miRNA sponge activity in primary cortical neurons following AAV-mediated miRNA sponge expression. Scale as indicated. (C) Quantitation of inhibition of tdTomato expression by miRNA sponge in primary cortical neuron. N = 19 – 26 neurons from 3 independent experiments. *$p<0.0001$. Two-tailed t-test with Welch's correction. Data shown as mean ± SEM.

Tables: Table 1: Data

Fig 1:		
HFD –enriched miRNAs	log_2 (Fold Change)	p-value (FDR)
miR-382	11.394	0.021
miR-1894	11.023	0.03
miR-196a	6.744	0.012
miR-145	7.219	0.024
let-7b	6.68	0.026
NCD –enriched miRNAs	log_2 (Fold Change)	p-value (FDR)
let-7e	-3.86	0.049
let-7i	-4.516	0.003
let-7d	-7.578	0.007

Fig 2:		
GO Terms	log_2 (Fold Enrichment)	log_{10} (FDR)
Regulation of synapse organization	2.653060017	1.306273051
Cellular response to hormone stimulus	2.411426246	1.353596274
Regulation of cell migration	1.794935663	1.410050399
Neuron differentiation	1.713695815	1.447331784
Calcium-dependent activation of synaptic vesicle fusion	6.64385619	1.457174573
Trans-synaptic signaling by BDNF	6.64385619	1.515700161
Regulation of cell differentiation	1.50589093	1.517126416
Response to hormone	2.15704371	1.530177984
Cell differentiation	1.077242999	1.590066877
Trans-synaptic signaling by BDNF, modulating synaptic transmission	6.64385619	1.607303047
Mitotic cell cycle phase transition	3.399171094	1.630784143
Trans-synaptic signaling by neuropeptide, modulating synaptic transmission	6.64385619	1.869666232
Regulation of neuron migration	4.432959407	1.931814138
Anaphase-promoting complex-dependent catabolic process	5.730639956	1.995678626
Pathways	log_2 (Fold Enrichment)	log_{10} (FDR)
Oxytocin receptor mediated signaling pathway	3.993674362	2.165579296
Gonadotropin-releasing hormone receptor pathway	2.761285273	2.165579296
Synaptic vesicle trafficking	4.457462965	1.698970004
Insulin/IGF pathway-mitogen activated protein kinase kinase/MAP kinase cascade	4.186659017	1.595166283
Insulin/IGF pathway-protein kinase B signaling cascade	4.067810784	1.562249437
FGF signaling pathway	2.94673086	1.54668166
Ionotropic glutamate receptor pathway	3.730096466	1.395773947
Nodes (Hubs)	Participation Coefficient	Z-Score

IGF1	0.206	3.37
CAMK2B	0.476	3.2
NTRK2	0.382	2.68
ERBB4	0.374	2.33
ANAPC11	0.214	2.35

Fig 3:			
IGF1 3'UTR			
	Mean Difference	SEM Difference	p-value
Control Sponge vs miRNA Sponge	0.937	0.3469	0.035
CAMK2B 3'UTR			
	Mean Difference	SEM Difference	p-value
Control Sponge vs miRNA Sponge	1.211	0.4275	0.014
NTRK2 3'UTR			
	Mean Difference	SEM Difference	p-value
Control Sponge vs miRNA Sponge	2.504	0.845	0.021
ERBB4 3'UTR			
	Mean Difference	SEM Difference	p-value
Control Sponge vs miRNA Sponge	1.461	0.5733	0.0282
ANAPC11 3'UTR			
	Mean Difference	SEM Difference	p-value
Control Sponge vs miRNA Sponge	0.4821	0.2916	0.15
Fig 4:			
AgRP BrdU			
	Mean Difference	SEM Difference	p-value
NCD vs HFD	59.59	19.88	0.004
POMC BrdU			
	Mean Difference	SEM Difference	p-value
NCD vs HFD	83.35	27.33	0.004
Fig 5:			
AgRP tdTomato			
	Mean Difference	SEM Difference	p-value
NCD + miRNA Sponge vs HFD + miRNA Sponge	41.91	3.801	<0.0001
POMC tdTomato			
	Mean Difference	SEM Difference	p-value
NCD + miRNA Sponge vs HFD + miRNA Sponge	3.017	2.630	0.262
Fig 6:			
c-Fos BrdU			
	Mean Difference	SEM Difference	p-value
NCD vs HFD	58.84	13.69	<0.0001
c-Fos BrdU			
	Mean Difference	SEM Difference	p-value
NCD + miRNA Sponge vs HFD + miRNA Sponge	57.50	3.545	<0.0001

Fig 7:			
AgRP c-Fos			
	Mean Difference	SEM Difference	p-value
NCD vs HFD	43.89	2.915	<0.0001
POMC c-Fos			
	Mean Difference	SEM Difference	p-value
NCD vs HFD	28.89	3.376	<0.0001
Fig 8:			
P75 Average Weight Gain (gms)			
	Mean Difference	SEM Difference	p-value
NCD vs HFD	1.002	0.1909	<0.0001
HFD vs HFD + miRNA Sponge	1.082	0.2052	<0.0001
Fat Mass Quantification (mg)			
	Mean Difference	SEM Difference	p-value
NCD vs HFD	3.428	0.897	0.0003
HFD vs HFD + miRNA Sponge	2.114	0.897	0.0217